

## Review

# Cathode materials for single-phase solid-solid conversion Li-S batteries

Jung Tae Kim,<sup>1,2</sup> Xiaoge Hao,<sup>1,2</sup> Changhong Wang,<sup>1,\*</sup> and Xueliang Sun<sup>1,\*</sup>

## SUMMARY

Widespread adoption of lithium-sulfur batteries (LSBs) remains inhibited, given their unrealized energy densities, drastic capacity fade, and severe self-discharge stemming from the polysulfide shuttle effect. Although countless endeavors have attempted to overcome this key bottleneck, “shuttle-free” lithium-sulfur batteries (SfLSBs) that operate by single-phase solid-solid conversion are a preeminent technology with vast potential to facilitate universal adoption of LSBs. In this review, we first provide a fundamental understanding of SfLSBs by comparing their operating mechanism with traditional LSBs. Then we present various strategies that have been used to enable SfLSBs in the liquid and solid state, placing particular emphasis on cathode materials. Finally, perspectives ranging from fundamental research to practical engineering design are provided to bolster future endeavors regarding SfLSB technology.

## INTRODUCTION

The paradigm shift toward renewable energy sources has resulted in development of various next-generation technologies reliant on clean energy.<sup>1</sup> In recent years, the global surge of battery-powered electric vehicles (EVs) has revolutionized the transportation industry, mitigating several environmental concerns inherent to gasoline-powered vehicles. Lithium-ion batteries (LIBs) are an essential component of EVs that dictates their range, charging time, cost, and safety.<sup>2,3</sup> Although LIBs have played a vital role in facilitating the transition toward fully electric transportation modes, the 30-year-old technology is on the verge of reaching its theoretical energy maximum and suffers from safety concerns that stem from using highly flammable organic liquid electrolytes.<sup>4,5</sup> Conventional LIBs rely on expensive and environmentally limited materials, such as nickel and cobalt, whose use faces additional scrutiny because of their uneven geographical distribution, supply chain instability, and unethical mining practices.<sup>6–8</sup> Among various next-generation batteries currently being developed, lithium-sulfur batteries (LSBs) have been identified as a promising alternative energy storage solution to LIBs. LSBs boast a high theoretical energy density of 2,600 Wh/kg and utilize non-toxic, abundant sulfur as the active material.<sup>9–12</sup> Although the advantages of LSBs are clear, they suffer from challenges such as (1) the low electrical conductivity of sulfur ( $1.0 \times 10^{-30}$  S cm<sup>-1</sup>) and its discharge product Li<sub>2</sub>S ( $1.0 \times 10^{-13}$  S cm<sup>-1</sup>), (2) severe volume change of sulfur during (de)lithiation, and (3) poor volumetric energy density.<sup>13</sup> A considerable challenge that hinders LSB technology stems from gradual dissolution of lithium polysulfide (LiPS) intermediates into the liquid electrolyte, which results in “shuttling” of active materials between the cathode and anode, a phenomenon otherwise referred to as the shuttle effect.<sup>14</sup> The shuttle effect has been identified as a critical bottleneck that limits LSB production because it results in low

## PROGRESS AND POTENTIAL

The global transition toward environmentally sustainable transportation modes, such as electric vehicles, has resulted in surging demand for safe, highly energy-dense, and economically feasible energy storage systems. “Shuttle-free” lithium-sulfur batteries (SfLSBs) that operate by single-phase solid-solid conversion have been identified as a promising energy storage solution. In this review, we discuss cathode materials for SfLSBs in both the liquid and solid state to bolster their progress and provide inspiration for developing energy storage technology based on sulfur chemistry for next-generation applications and devices.



Coulombic efficiency, a short cycle life, unrealized energy density, and self-discharge.

Over the past decade, countless efforts have been made to suppress the shuttle effect. A prominent approach has been to encapsulate sulfur in porous carbon hosts, such as carbon nanotubes, carbon spheres, and graphene.<sup>15–17</sup> The carbon hosts can prevent LiPS dissolution by physical and chemical absorption and mitigate the shuttle effect as a result.<sup>18</sup> Traditional carbon materials, however, often have poor affinity toward LiPS intermediates and cannot fully prevent their dissolution into the electrolyte.<sup>19</sup> Thus, another strategy to suppress the shuttle effect has been to incorporate electrocatalytic materials into the cathode composite.<sup>20–24</sup> By doing so, the LiPS intermediates quickly convert into the electrolyte-insoluble products  $\text{Li}_2\text{S}_2$  and  $\text{Li}_2\text{S}$ . Although this is a fruitful strategy, the shuttle effect is still only mitigated rather than completely prevented. A strategy that can directly address the shuttle effect is to alter the electrochemical reaction pathway of LSBs so that they exhibit single-phase solid-solid conversion from S to  $\text{Li}_2\text{S}$ . By doing so, dissolution of LiPS intermediates is completely avoided, and the shuttle effect is directly addressed. Single-phase solid-solid conversion LSBs, referred to in this review as “shuttle free” LSBs (SfLSBs), have a long cycling life, high Coulombic efficiency, low self-discharge rate, high energy density, and excellent safety.<sup>25–27</sup> In the liquid state, SfLSBs have been achieved through different cathode configurations and in the solid state by replacing the liquid electrolyte with a solid-state electrolyte (SSE). These strategies directly address the shuttle effect and are a promising approach to realizing practical LSBs.<sup>28</sup> Despite numerous studies reporting SfLSBs, a comprehensive review that emphasizes cathode composite material design and engineering is lacking.

In this review, we provide a fundamental understanding of SfLSBs by comparing their operating mechanism with traditional LSBs. Then we present various strategies that have been used to achieve SfLSBs in the liquid state, focusing on sulfur cathode composites based on sulfurized polyacrylonitrile (S-PAN), sulfur molecule confinement, and chemical stabilization via metal/non-metal doping. A transition is then made to describing all-solid-state LSBs, which have innate shuttle-free characteristics, using recent contributions to highlight the design and fabrication of metal-sulfide, lithium-sulfide, and sulfur-based cathode composites. Finally, we provide perspectives ranging from fundamental research to practical engineering design for the liquid- and solid state to bolster development of SfLSBs. With this review, we hope to shed light on the SfLSB system and provide inspiration for developing next-generation batteries based on sulfur chemistry.

### Fundamental operating mechanism of SfLSBs

The multi-phase redox chemistry of a typical LSB is shown by the voltage profile in Figure 1A. During discharge, sulfur reacts with incoming electrons and ions to form long-chain LiPSs ( $\text{Li}_2\text{S}_x$ ,  $4 \leq x \leq 8$ ), short-chain LiPSs ( $\text{Li}_2\text{S}_x$ ,  $2 < x \leq 4$ ), and finally the discharge products  $\text{Li}_2\text{S}_2/\text{Li}_2\text{S}$  through solid-liquid-solid conversion. Long-chain LiPSs are highly soluble in organic liquid electrolytes and diffuse from the cathode to the anode during cell operation, resulting in loss of active materials, degradation of the lithium anode, poor utilization of sulfur, and severe self-discharge, all factors that degrade battery performance.<sup>29,30</sup> In contrast, an LSB that operates by single-phase solid-solid conversion from S to  $\text{Li}_2\text{S}$  prevents dissolution of LiPSs and completely avoids the shuttle effect. The voltage profile of an SfLSB is shown in Figure 1B. Here, the single plateau is characteristic of single-phase sulfur redox chemistry, corresponding to formation of  $\text{Li}_2\text{S}$  during discharge.

<sup>1</sup>Department of Mechanical & Materials Engineering, University of Western Ontario, London, ON N6A 5B9, Canada

<sup>2</sup>These authors contributed equally

\*Correspondence: [cwang622@uwo.ca](mailto:cwang622@uwo.ca) (C.W.), [xsun9@uwo.ca](mailto:xsun9@uwo.ca) (X.S.)

<https://doi.org/10.1016/j.matt.2022.11.019>

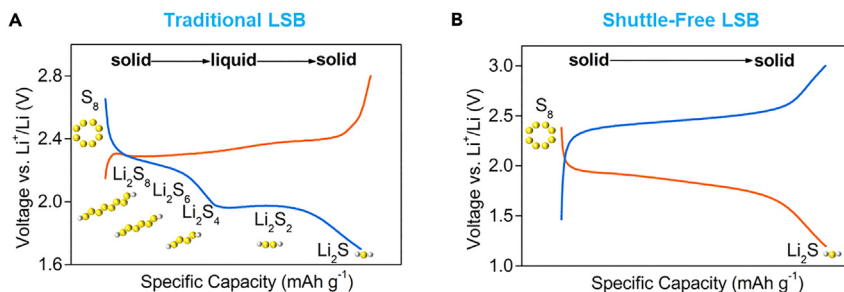


**Figure 1. Voltage profiles of traditional and SfLSBs**

(A) Multi-phase solid-liquid-solid conversion.  
(B) Single-phase solid-solid conversion.

Solid-solid conversion SfLSBs have been widely reported for liquid- and solid-state configurations. For liquid SfLSBs, preventing dissolution of LiPSs is crucial for circumventing the shuttle effect. In this regard, cathode composite material design and engineering play a vital role. For solid-state SfLSBs, dissolution of LiPSs is no longer a concern, and the cathode composite material does not influence the solid-solid conversion pathway like in liquid SfLSBs. Still, the role of cathode materials cannot be underplayed because they directly influence the electrochemical behavior of LSBs.

In the following sections, we delve deeper into SfLSB technology by focusing on different sulfur cathode composites used in the liquid- and solid-state system. The liquid state is categorized into four main sections: (1) S-PAN, (2) sulfur molecule confinement, (3) metal/non-metal doping, and (4) other strategies. The solid-state consists of three main sections: (1) metal-sulfide cathodes, (2) lithium-sulfide cathodes, and (3) sulfur cathodes. Tables that summarize parameters such as cathode composite composition and sulfur loading used in recent studies are also provided to guide future endeavors.

## VARIOUS SULFUR CATHODES WITH SHUTTLE-FREE CHARACTERISTICS IN LIQUID Li-S BATTERIES

### Chemical bonding via S-PAN

S-PAN represents a class of cathode material that has attracted considerable interest for rechargeable LSBs because of its low cost, excellent thermal stability, and high electronic conductivity.<sup>31–33</sup> In 2002, Wang et al.<sup>34</sup> first demonstrated the effectiveness of S-PAN composite cathodes for LSBs. S-PAN was synthesized by heating commercial sulfur and PAN powder at 280°C–300°C in an argon atmosphere for 6 h (Figure 2A).<sup>34</sup> During the synthesis process, sulfur acts as a dehydrogenation agent and effectively dehydrogenates PAN, initiating cyclization of its polymer chains to form a conductive heterocyclic composite material containing uniformly embedded sulfur atoms. Since their introduction, S-PAN composite cathodes have gained considerable interest for LSB applications because they enable single-phase solid-solid conversion that can effectively circumvent the shuttle effect by chemically bonding LiPSs onto the carbon skeleton. The single-phase solid-solid conversion mechanism can be attributed to the two-electron reaction that occurs during oxidation and reduction (Figure 2B).<sup>35</sup> During S-PAN synthesis, the C≡N bonds of PAN convert into C=N bonds to form a cyclized structure. The S-S bonds in sulfur then break to form C-S and S-S bonds in the side chain of PAN, allowing short-chain sulfur molecules to graft and anchor into the cyclized structure. The reaction mechanism of S@C and S-PAN composite cathodes differ greatly, and this

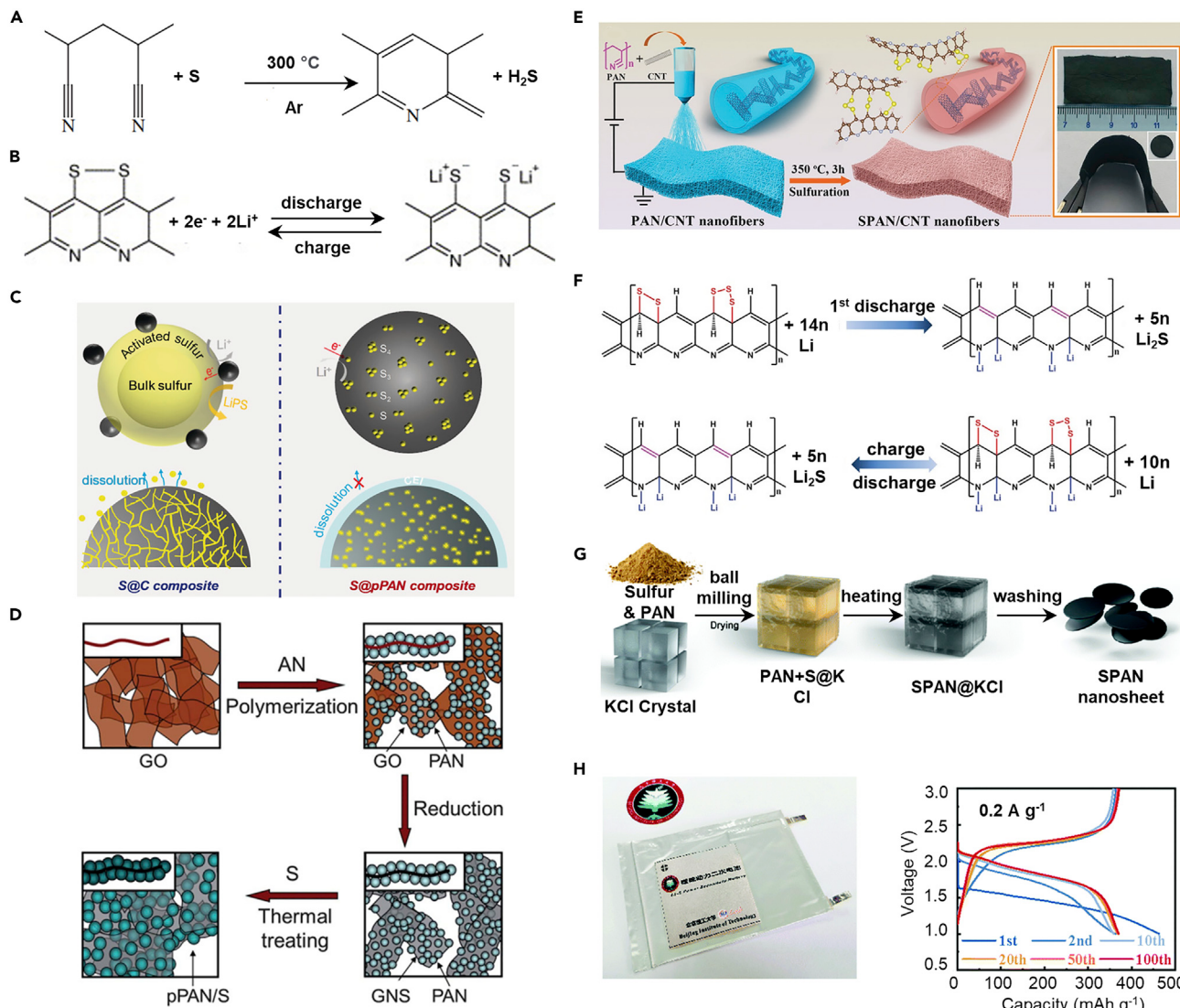


**Figure 2. Sulfurized-polyacrylonitrile (S-PAN) cathode composites for SfLSBs**

(A) Schematic showing the basic synthesis route for S-PAN. Reproduced with permission from Wang et al.<sup>34</sup> Copyright 2002, Wiley.

(B) Two-electron reaction mechanism of S-PAN that enables solid-solid conversion in LSBs. Reproduced with permission from Yu et al.<sup>35</sup> Copyright 2004, Elsevier.

(C) Reaction mechanism of traditional S@C cathodes in ether-based solvents and S-PAN cathodes in carbonate-based solvents. Reproduced with permission from Yang et al.<sup>36</sup> Copyright 2020, Wiley.

(D) 2D PAN/graphene nanosheet (GNS) cathode composite fabricated by an *in situ* polymerization method. Reproduced with permission from Yin et al.<sup>42</sup> Copyright 2012, Royal Society of Chemistry.

(E) Fabrication process of electrospun S-PAN/CNT cathode composites. Reproduced with permission from Wang et al.<sup>43</sup> Copyright 2019, Wiley.

(F) The proposed electrochemical lithiation/delithiation mechanism of the electrospun S-PAN/CNT cathode composites. Reproduced with permission from Wang et al.<sup>43</sup> Copyright 2019, Wiley.

(G) Synthesis route for S-PAN nanosheets. Reproduced with permission from Wang et al.<sup>44</sup> Copyright 2021, Royal Society of Chemistry.

(H) Digital photograph of a Li-S-PAN pouch cell using S-PAN nanosheets and the corresponding voltage profile at different cycles. Reproduced with permission from Wang et al.<sup>44</sup> Copyright 2021, Royal Society of Chemistry.

has been extensively documented in a recent review.<sup>36</sup> A distinct feature of S-PAN is gradual formation of LiPSs during charge/discharge that chemically bond to the surface of the conductive polymer matrix. The formed LiPSs react with the carbonate electrolyte to form a cathode electrolyte interphase (CEI) layer (Figure 2C). Formation of the CEI layer ensures that the active sulfur species are fixed to the S-PAN

particles, preventing their migration and/or segregation. Wang et al.<sup>37</sup> exemplified the importance of the CEI layer by replacing ethylene carbonate (EC) with fluoroethylene carbonate (FEC) in carbonate electrolytes to facilitate formation of a LiF-rich CEI layer on S-PAN. The LiF-rich CEI film prevents LiPS diffusion from the inner to the outer surface, enabling an LSB that can run for 4,000 cycles under 6 C with a capacity retention of 96.8%.<sup>37</sup> Because S-PAN composite cathodes operate by a single-phase solid-solid reaction mechanism rather than the dissolution-deposition mechanism in traditional S@C cathodes, they can achieve stable operation in carbonate electrolytes.<sup>38–41</sup>

Over the past decade, many efforts have been made to enhance the electrochemical performance of S-PAN composite cathodes. For instance, Yin et al.<sup>42</sup> designed a PAN/graphene nanosheet (GNS) composite using an *in situ* polymerization method (Figure 2D). The pPAN-S/GNS composites exhibited enhanced cycling stability and rate performance in comparison with bare S-PAN. The highly conductive GNS provides a robust substrate that can alleviate the volume change of sulfur, prevent agglomeration of sulfur nanoparticles, and shorten the Li<sup>+</sup>/e<sup>-</sup> conduction pathway. In ether-based solvents, S-PAN composite cathodes still suffer from the shuttle effect, resulting in fast capacity fade and poor electrochemical performance.<sup>35,45,46</sup> To tackle this issue, Wang et al.<sup>43</sup> fabricated a conductive 3D network of electrospun S-PAN nanofibers with carbon nanotubes (S-PAN@CNT) in a two-step process (Figure 2E). This electrode architecture enables a strong interaction between the PAN backbone and short-chain sulfur molecules (S<sub>x</sub>, x = 2,3), resulting in stable cell operation in ether and carbonate electrolytes. The voltage profile for both electrolytes shows a single plateau, indicating single-phase solid-solid conversion. LiPS signals are absent in the NMR and UV absorption spectra, providing evidence of the single-step sulfur redox pathway.<sup>43</sup> The electrochemical lithiation/delithiation mechanism of the as-prepared S-PAN cathodes suggests that sulfur undergoes single-phase solid-solid conversion (Figure 2F). Recently, a salt-templating method was used to fabricate ultrathin S-PAN nanosheets (Figure 2G).<sup>44</sup> The high surface area of the S-PAN nanosheets enables better electrolyte wettability, shortening the redox pathway and improving the reaction kinetics. When evaluated in pouch cells, the S-PAN nanosheets deliver a capacity retention of nearly 100% for 100 cycles, demonstrating their practical viability (Figure 2H). The voltage profiles exhibit a single plateau, indicating the shuttle-free capability of S-PAN, even in a pouch cell configuration.

S-PAN cathodes have shown great promise for enabling LSB technology. However, their practical application still requires improvement. Currently, the precise structure of S-PAN remains unclear, especially because its structure changes during cycling.<sup>47</sup> Studies that utilize *in situ* characterization techniques such as Raman spectroscopy, X-ray photoelectron spectroscopy (XPS), and X-ray absorption near-edge structure (XANES) are crucial for understanding the structure of S-PAN composite cathodes and their failure mechanism during cell operation. Low sulfur content is another challenge that needs to be addressed for S-PAN cathodes. This requires new structural designs that can accommodate high sulfur loadings above 60 wt % while still maintaining the shuttle-free characteristics of S-PAN cathodes. In terms of their practical application, future work should focus on testing S-PAN cathodes in a pouch cell configuration because the cycle life of typical Ah-level Li-S pouch cells is currently very poor (<100 cycles).<sup>48</sup> This will help bridge the gap between laboratory research and industrial-scale production of LSBs based on S-PAN composite cathodes.<sup>49,50</sup> Finally, the low density of S-PAN limits the volumetric energy density of LSBs, which is a crucial factor for EV applications. The volumetric energy density can be increased

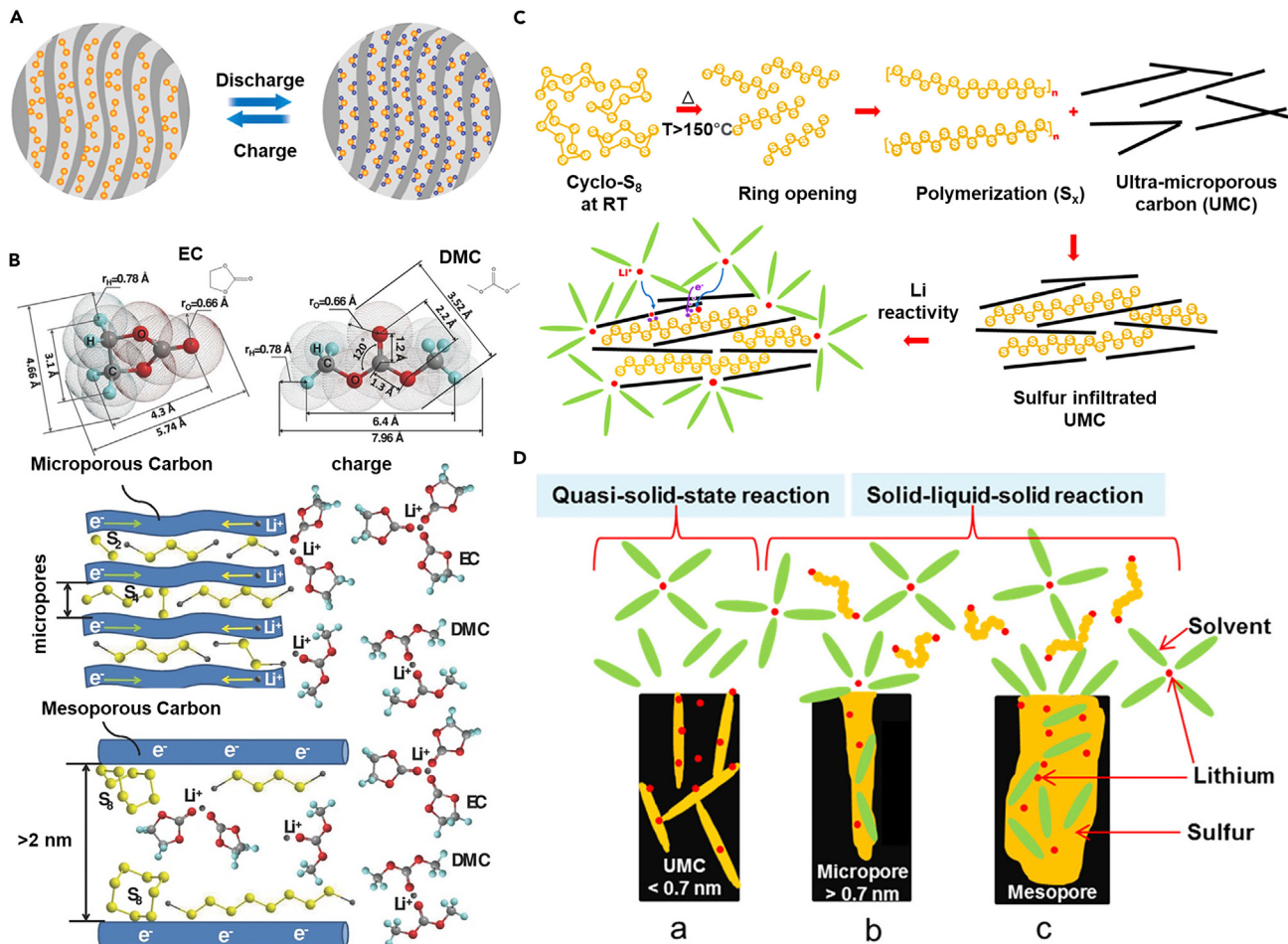


**Figure 3. Sulfur confinement strategies to enable single-phase solid-solid conversion LSBs**

(A) Schematic showing sulfur-carbon composite cathodes with metastable sulfur allotropes. Reproduced with permission from Xin et al.<sup>55</sup> Copyright 2012, American Chemical Society.

(B) Geometric dimensions of EC and diethylene carbonate molecules, used to illustrate and compare the lithiation process of microporous sulfur-carbon cathodes with mesoporous sulfur-carbon cathodes in carbonate-based solvents. Reproduced with permission from Li et al.<sup>56</sup> Copyright 2014, Wiley.

(C) Preparation method of ultramicroporous-sulfur cathode composites under a vacuum. Reproduced with permission from Helen et al.<sup>57</sup> Copyright 2018, American Chemical Society.

(D) Schematic comparing the reaction pathway of carbon-sulfur composites with varying carbon pore sizes. Reproduced with permission from Helen et al.<sup>57</sup> Copyright 2018, American Chemical Society.

by reducing the amount of carbon and binder in the cathode composite and by incorporating materials with higher tap density, such as selenium.<sup>38,51–54</sup>

#### Molecular confinement of sulfur molecules

A decade after introduction of S-PAN, Xin et al.<sup>55</sup> discovered a new sulfur-carbon composite cathode based on the metastable sulfur allotropes  $S_{2-4}$  ( $S_2$ ,  $S_3$ , and  $S_4$ ), which operate by a single-phase solid-solid conversion mechanism (Figure 3A). The cathodes were fabricated by coating commercial CNTs with a microporous carbon (MPC) matrix through a simple solution-based method. A conventional melt-diffusion technique was then used to impregnate sulfur and obtain S/CNT@MPC cathode composites. The narrow pores (~0.5 nm) in the MPC layer act as small reservoirs so that they can only accommodate the short-chain sulfur molecules  $S_{2-4}$ .

during the discharge/charge process, completely avoiding the conversion of  $S_8$  to  $S_4^{2-}$  and resulting in the single-plateau curve in the voltage profile corresponding to the single-phase solid-solid conversion mechanism. The S/CNT@MPC cathodes can achieve stable performance in ether and carbonate electrolytes, exhibiting a reversible capacity above 1,000 mAh g<sup>-1</sup> for over 200 cycles. Then it was reported that the microstructure of the carbon matrix considerably influences the solid-solid redox behavior of  $S_{2-4}$  cathodes.<sup>56</sup> The nanosized pores of ordered mesoporous carbon (FUD) blocks direct contact between sulfur species and carbonate molecules because the pore size (~0.46 nm) is much smaller than the diameter of EC (5.74 Å) and dimethyl carbonate (7.96 Å) molecules (Figure 3B). The physical barrier the pores provide helps prevent irreversible reactions between carbonate molecules and sulfur species, enabling stable operation in carbonate electrolytes. The pores of FUD also blocked infiltration of ether molecules, hindering dissolution of LiPSs in ether electrolytes. Consequently, the electrochemical behavior of FUD/S-40 ( $S_{2-4}$ ) cathodes (i.e., single discharge plateau, good cycling stability) were similar in carbonate and ether-based solvents.

For some time, the existence of small sulfur molecules was assumed to be a necessary condition for LSBs to proceed by a single-phase solid-solid conversion pathway. However, this notion has been largely refuted because this distinct redox behavior has also been observed in other sulfur species. Helen et al. discovered that linear polymeric sulfur confined in an ultramicroporous carbon (UMC) matrix could promote a single-phase solid-solid conversion pathway (Figure 3C).<sup>57</sup> Although sulfur exists in a linear polymeric state rather than smaller allotropes, the micropores of the UMC (<0.7 nm) can effectively prevent the solvent molecules from penetrating the matrix (Figure 3D). This work also suggests that the spatial constraints (i.e., pore size) of the carbon source are key factors for enabling single-phase solid-solid conversion LSBs. Still, systematic studies are needed to elucidate the relationship between the pore size and the single-phase solid-solid conversion pathway in LSBs because the working mechanism remains ambiguous.

It is important to note the dilemma that arises when employing microporous carbon matrices. Confining sulfur species in a carbon matrix with small pore size is an effective way to circumvent the shuttle effect and prevent irreversible side reactions in carbonate-based solvents. However, when the pore size of the carbon matrix is small, achieving high sulfur loading is difficult. This is impractical for obtaining LSBs with high energy density. Future work should focus on elucidating the relationship between pore size and different sulfur molecules. New microporous cathode designs that can accommodate high sulfur content (>60 wt %) without sacrificing cycling stability in carbonate-based solvents should be developed. Both thrusts will help guide materials design for LSBs that apply a sulfur molecular confinement strategy.

#### Chemical stabilization of sulfur species via metal/non-metal doping

Chemical stabilization of sulfur species via metal/non-metal doping is another strategy that has been used to achieve SfLSBs in the liquid state. For instance, copper-stabilized sulfur-microporous carbon composites (MC-Cu-S) were synthesized by dispersing highly conductive copper (Cu) nanoparticles into a microporous carbon host and wet-impregnating sulfur (Figure 4A).<sup>58</sup> The Cu nanoparticles chemically interact with sulfur species to form stable Cu-S/LiPS clusters, effectively circumventing dissolution of LiPS intermediates and enabling stable operation in carbonate-based electrolytes. Even at a relatively high sulfur loading of 50 wt %, the MC-Cu-S cathodes operate in the absence of the shuttle effect, demonstrating

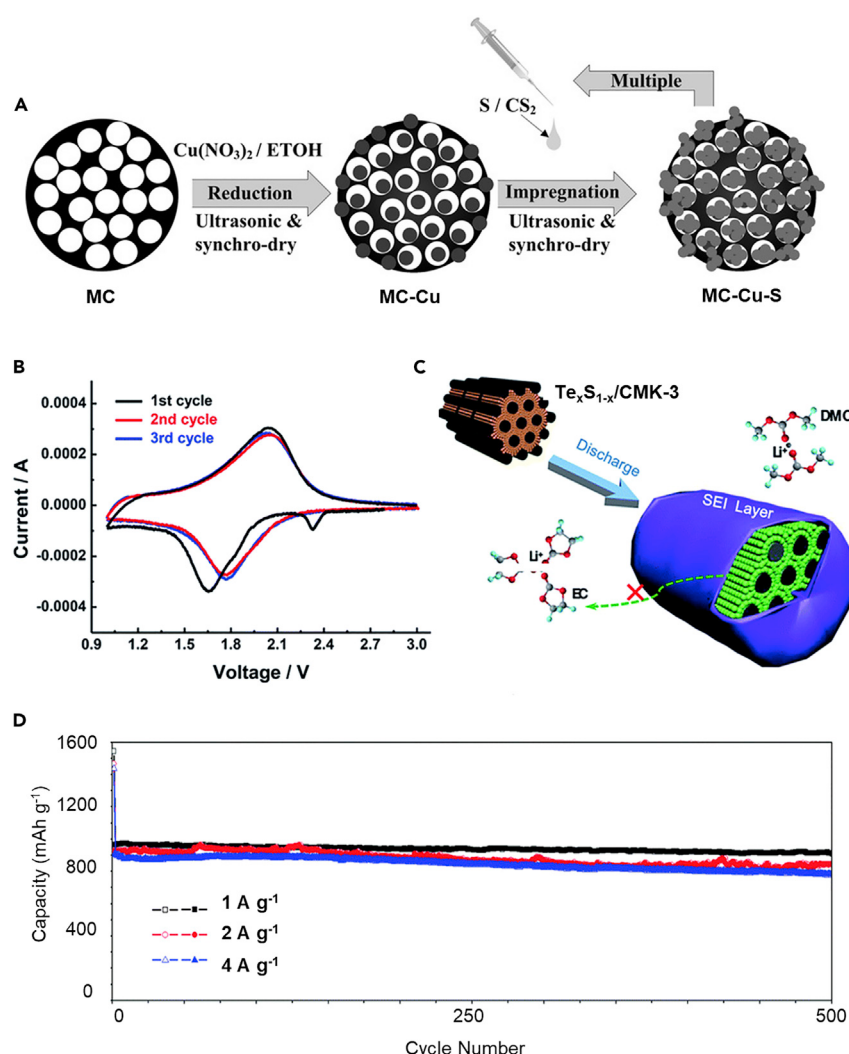


**Figure 4. Shuttle-free sulfur cathodes via metal/non-metal chemical stabilization**

(A) Fabrication process for Cu-stabilized sulfur-microporous carbon composites. Reproduced with permission from Zheng et al.<sup>58</sup> Copyright 2014, Wiley.

(B) CV curves of synthesized heteroatomic  $\text{Te}_x\text{S}_{1-x}$  molecule/CMK-3 nanocomposites. Reproduced with permission from Sun et al.<sup>59</sup> Copyright 2018, Royal Society of Chemistry.

(C) Schematic of Te-induced SEI layer formation on  $\text{Te}_x\text{S}_{1-x}$  molecule/ CMK-3 nanocomposites. Reproduced with permission from Sun et al.<sup>59</sup> Copyright 2018, Royal Society of Chemistry.

(D) Cycling performance of  $\text{S}_{0.94}\text{Se}_{0.06}/\text{C}$  electrodes at different current densities. Reproduced with permission from Li et al.<sup>60</sup> Copyright 2015, Royal Society of Chemistry.

the effectiveness of metal stabilization for achieving SfLSBs. In a similar approach, a mixed Te-S cathode was fabricated by confining heteroatomic  $\text{Te}_x\text{S}_{1-x}$  ( $x = 0.05, 0.1$ , and  $0.2$ ) molecules into mesoporous carbon (CMK-3) using a melt-diffusion technique.<sup>59</sup> Formation of Te-S bonds stabilizes sulfur species in the CMK-3 matrix, effectively reducing dissolution of LiPS intermediates. The small cathodic peak that appears at  $\sim 2.3$  V in the cyclic voltammetry (CV) curves completely disappears in the subsequent cycles (Figure 4B). This is attributed to formation of an SEI layer that coats the electrode surface because of side reactions between the polytellurides and polysulfotellurides with the carbonate electrolyte in the first cycle (Figure 4C). Although formation of the SEI layer results in unwanted electrolyte consumption,

it can prevent more side reactions between the electrolyte and active species from occurring and stabilize the electrode interface so that the shuttle effect is completely avoided. Li et al.<sup>60</sup> proposed amorphous S-rich  $S_{1-x}Se_x/C$  composites to achieve single-phase solid-solid phase conversion in LSBs. During the first discharge process, a small plateau at about 2.5 V can be seen, indicating slight dissolution of polysulfides into the electrolyte. However, only one discharge/charge plateau around 2.0 V is observed in the following cycles, suggesting that selenium introduction can effectively circumvent the shuttle effect. The Se-S cathodes deliver stable capacities for over 500 cycles, even at high rates, demonstrating the effectiveness of sulfur stabilization by trace selenium doping (Figure 4D). Similar cathode composites based on Se-S and Te-S have been applied to all-solid-state LSBs, which will be discussed in a following section.

These contributions have demonstrated the effectiveness of metal/non-metal stabilization for achieving single-phase solid-solid conversion in sulfur cathodes. Introduction of metals/non-metals results in enhanced reaction kinetics of the cathode composite.<sup>52–54,60–62</sup> Improving the reaction kinetics is especially important for SfLSBs because solid-solid conversion is known to be the rate-limiting step in LSBs. Along with metal/non-metal doping, catalysis is another promising strategy to improve the reaction kinetics of solid-solid conversion LSBs and should be explored in future studies.<sup>20,23,24,28</sup> Introduction of metals/non-metals also increases the density of sulfur, which greatly improves the volumetric energy density of LSBs. Future studies should explore low-cost transition metals to maximize the cost advantage of LSBs. At the same time, different synthesis methods should be developed to realize mass production to bolster the practical application of LSBs based on metal/non-metal-stabilized S-based cathodes.

### Other strategies to achieve SfLSBs

Recent contributions have demonstrated new cathode architectures and strategies that can achieve SfLSBs. For example, Zhang et al.<sup>63</sup> reported organosulfur/CNT hybrid cathodes that proceed by a single-phase solid-solid conversion in ether-based electrolytes (Figure 5A). A sulfur-chain-controlling strategy is used to manipulate the chain length of sulfur in disulfide polymers (DSPs) and trisulfide polymers (TSPs). The non-sulfur organic units and C-S bonds in the sulfur-rich polymers can effectively circumvent the shuttle effect by chemical absorption and covalent fixing. Even at a high sulfur loading of over 76 wt %, TSPs operate by single-phase solid-solid conversion and effectively avoid the shuttle effect when employed in an ether-based electrolyte. In an alternative approach, a superconcentrated dual-salt carbonate electrolyte was used to form a solid electrolyte interphase (SEI) layer on the surface of a sulfur/mesoporous carbon composite material (S/CMK-3).<sup>64</sup> As depicted in Figure 5B, the superconcentrated electrolyte induces formation of an SEI layer that can block migration of LiPS intermediates and solvent molecules. At a high sulfur loading of 65 wt %, the S/CMK-3 composites deliver a reversible capacity of 1,009 mAh g<sup>-1</sup>, demonstrating the importance of SEI design by electrolyte tuning. In another approach, molecular layer deposition (MLD) was used to deposit a nanoscale alucone film onto a traditional carbon-sulfur composite electrode (Figure 5C).<sup>65</sup> The alucone film serves as a flexible protective layer that can (1) alleviate the volume change of sulfur during cycling and (2) prevent side reactions between LiPS intermediates and carbonate molecules. The alucone-coated C-S electrodes deliver a capacity of over 570 mAh g<sup>-1</sup> for 300 cycles in carbonate electrolyte (Figure 5D). This work demonstrates a universal MLD approach that can enable use of conventional carbon-sulfur cathode composites in carbon-based electrolytes without any re-design or modification of the composite materials themselves. In a following study, operando XANES was

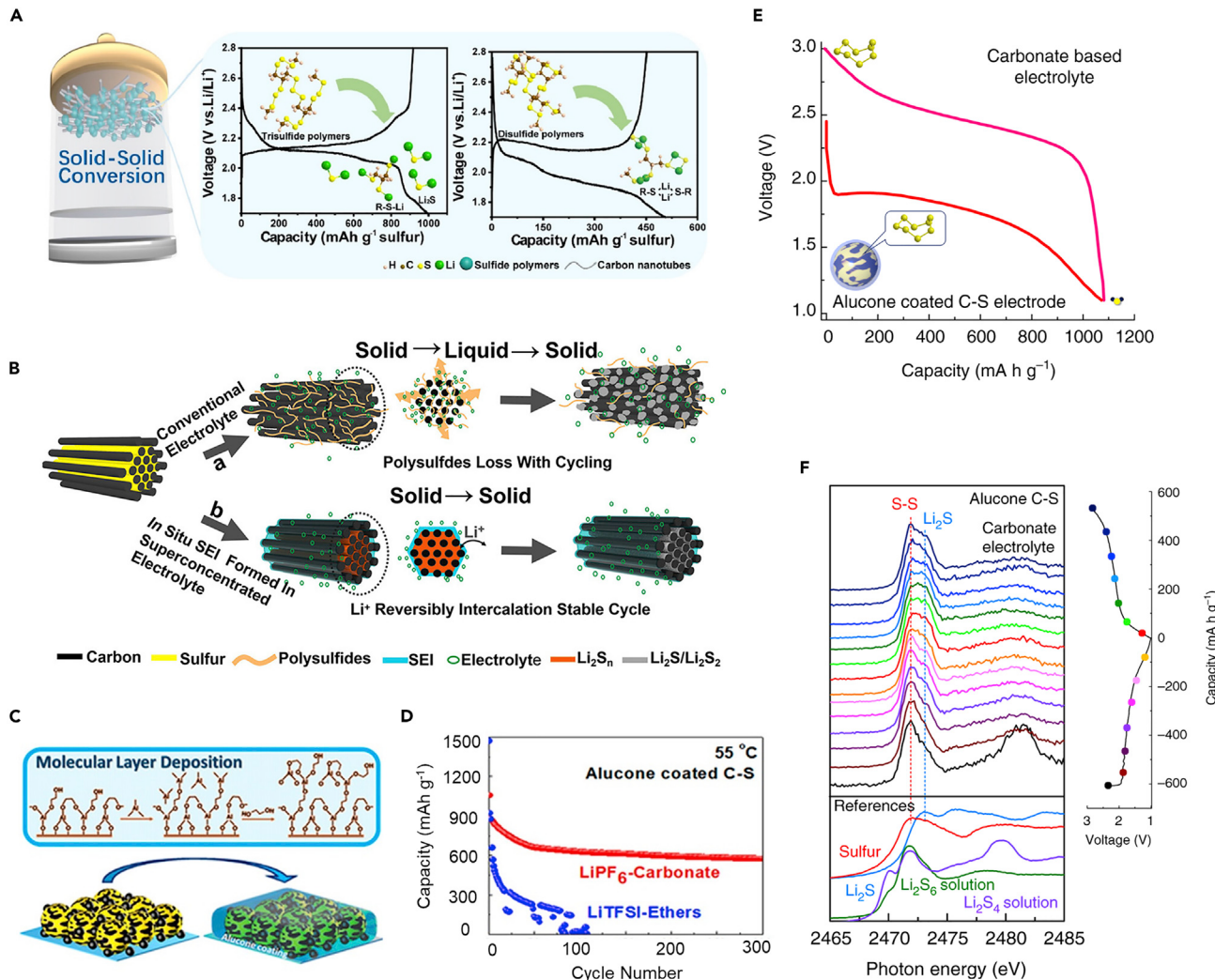


**Figure 5. Examples of other cathode configurations that operate by solid-solid conversion in LSBs**

(A) Organosulfur/CNT hybrid cathodes exhibiting shuttle-free characteristics in ether-based solvents. Reproduced with permission from Zhang et al.<sup>63</sup> Copyright 2022, Elsevier.

(B) Schematic showing *in situ* formation of an SEI layer on an S/CMK-3 cathode composite by using a superconcentrated dual-salt carbonate electrolyte system that enables a solid-solid conversion. Reproduced with permission from Chen et al.<sup>64</sup> Copyright 2019, American Chemical Society.

(C) Alucone coating deposited onto a traditional C@S cathode by molecular deposition technique. Reproduced with permission from Li et al.<sup>65</sup> Copyright 2016, American Chemical Society.

(D) Cycling performance of alucone-coated C@S cathodes in carbonate- and ether-based solvents at 55°C. Reproduced with permission from Li et al.<sup>65</sup> Copyright 2016, American Chemical Society.

(E) Voltage profile of alucone-coated C@S cathodes in carbonate-based solvent. Reproduced with permission from Li et al.<sup>66</sup> Copyright 2018, Nature Research.

(F) Operando XANES of alucone-coated C@S cathodes in ether-based solvents. Reproduced with permission from Li et al.<sup>66</sup> Copyright 2018, Nature Research.

used to reveal the underlying mechanism of the single discharge-charge plateau observed in alucone-coated C-S electrodes in carbonate electrolyte systems (Figure 5E).<sup>66</sup> The XANES results suggest single-phase solid-solid conversion, which indicates that cyclo-S<sub>8</sub>-based cathodes can also operate by this unique redox pathway (Figure 5F). These studies demonstrate other unique approaches that have been used to achieve single-phase solid-solid conversion LSBs, such as sulfur-chain control, high-concentration dual-salt electrolytes, and MLD modification.

**Table 1.** Literature review of cathodes with solid-solid conversion in liquid LSBs

Cathode composite	Electrolyte	Active material loading (mg cm <sup>-2</sup> )	Cycling performance	Reference
S-PAN	1 M LiPF <sub>6</sub> in EC/DMC (1:1, vol %)	N/A	600 mAh g <sup>-1</sup> /50 cycles	Wang et al. <sup>34</sup>
pPAN-S/GNS	1 M LiPF <sub>6</sub> in EC/DMC (1:1, vol %)	N/A	1,200 mAh g <sup>-1</sup> /0.1 C/100 cycles	Yin et al. <sup>42</sup>
S-PAN/CNT nanofibers	1 M LiPF <sub>6</sub> in EC/DMC (1:1, vol %) + 0.2 M LiNO <sub>3</sub>	2 mg cm <sup>-2</sup>	1,180 mAh g <sup>-1</sup> /800 mA g <sup>-1</sup> /800 cycles	Wang et al. <sup>43</sup>
S-PAN nanosheets	1 M LiPF <sub>6</sub> in EC/DMC (1:1, vol %)	5.8 mg cm <sup>-2</sup>	592.4 mAh g <sup>-1</sup> /0.2 A/300 cycles	Wang et al. <sup>44</sup>
S(CNT@MPC)	1 M LiPF <sub>6</sub> in EC/DMC (1:1, vol %)	1.0 mg cm <sup>-2</sup>	508 mAh g <sup>-1</sup> /0.1 C/200 cycles	Xin et al. <sup>55</sup>
FDU/S-40	1 M LiPF <sub>6</sub> in EC/DMC (1:1, vol %)	1 mg cm <sup>-2</sup>	>600 mAh g <sup>-1</sup> /400 mA g <sup>-1</sup> /500 cycles	Li et al. <sup>56</sup>
UMC-S	1 M LiTFSI in DOL/DME (1:1, vol %)	2 mg cm <sup>-2</sup>	~250 mAh g <sup>-1</sup> /0.05 C/60 cycles	Helen et al. <sup>57</sup>
MC-Cu-S	1 M LiPF <sub>6</sub> in EC/DMC (1:1, vol %)	1 mg cm <sup>-2</sup>	600 mAh g <sup>-1</sup> /100 mA g <sup>-1</sup> /500 cycles	Zheng et al. <sup>58</sup>
Te <sub>x</sub> S <sub>1-x</sub> /CMK-3	1 M LiPF <sub>6</sub> in EC/DMC (1:1, vol %)	2.5–2.9 mg cm <sup>-2</sup>	387 mAh g <sup>-1</sup> /3,000 mA g <sup>-1</sup> /500 cycles	Sun et al. <sup>59</sup>
S <sub>0.94</sub> Se <sub>0.06</sub> /C	1 M LiPF <sub>6</sub> in EC/DMC (1:1, vol %)	~0.8–1.5 mg cm <sup>-2</sup>	910 mAh g <sup>-1</sup> /1,000 mA g <sup>-1</sup> /500 cycles	Li et al. <sup>60</sup>
TSP/CNT	1 M LiTFSI in DME/DOL (1:1, vol %) + 0.2 M LiNO <sub>3</sub>	~0.6–0.8 mg cm <sup>-2</sup>	332 mAh g <sup>-1</sup> /1 C/600 cycles	Zhang et al. <sup>63</sup>
CMK-3/S	6 M LiTFSI in EC/DMC/EMC/FEC	~1.5–2.0 mg cm <sup>-2</sup>	871 mAh g <sup>-1</sup> /0.5 C/100 cycles	Chen et al. <sup>64</sup>
Alucone-coated KJ EC-600/S	1 M LiPF <sub>6</sub> + EC/EMC/DEC (1:1:1, vol %)	0.9 mg cm <sup>-2</sup>	429 mAh g <sup>-1</sup> /0.1 C/100 cycles	Li et al. <sup>65</sup>
Alucone-coated BP2000	1 M LiPF <sub>6</sub> in EC/DEC +10 wt % FEC	~1.2–4.0 mg cm <sup>-2</sup>	870 mAh g <sup>-1</sup> /320 mAh g <sup>-1</sup> /300 cycles	Li et al. <sup>66</sup>

As described above, there are several different strategies that can be used to achieve SfLSBs in the liquid state. Some of these approaches include chemical bonding via S-PAN, molecular confinement of sulfur, and sulfur stabilization via metal/non-metal doping. SfLSBs have distinct advantages over traditional LSBs, which include (1) avoidance of LiPS dissolution, (2) stable operation in carbonate electrolyte, (3) no self-discharge, (4) low electrolyte/sulfur (E/S) ratio, and (5) less Li anode corrosion. Although there are many advantages that stem from the single-phase solid-solid conversion pathway, challenges such as (1) low sulfur content, (2) poor sulfur utilization (particularly with high sulfur loading), and (3) sluggish solid-solid conversion hinder practical application of SfLSBs. Table 1 summarizes various performance parameters of liquid SfLSBs to guide future work.

## SOLID-STATE SfLSBs

The development of solid-state batteries (SSBs) has sparked a fascinating paradigm shift away from traditional liquid-based batteries, giving rise to a new era of energy storage technologies. The success of next-generation applications, such as electric planes and aerial drones, hinges on development of new battery chemistries that can satisfy the strict performance and safety requirements required for their commercialization.<sup>67</sup> Although they are still in their infancy, SSBs have potential to transcend traditional liquid-based systems in aspects ranging from energy density, charging time, and scalability to, most importantly, safety.<sup>68–70</sup> Although many SSB systems are being developed in parallel, solid-state LSBs (SSLSBs) have been considered to be among the best candidates for enabling SSB technology with energy densities over 500 Wh kg<sup>-1</sup>.<sup>71,72</sup> SSLSB technology remains nascent because there are many technical and scientific challenges that are similar to but also distinct from their liquid counterparts. Some similarities include the insulating nature of sulfur, severe volume expansion during (de)lithiation, and sluggish conversion kinetics.<sup>73,74</sup> In terms of the shuttle effect, dissolution of LiPSs is completely avoided in an all-solid-state configuration.<sup>74</sup> Consequently, SSLSBs are shuttle free intrinsically and operate by single-phase solid-solid conversion without any modification to the cathode. Still, cathode material design and fabrication has played a pivotal role in addressing several challenges hindering SSLSB technology. The following sections provide a

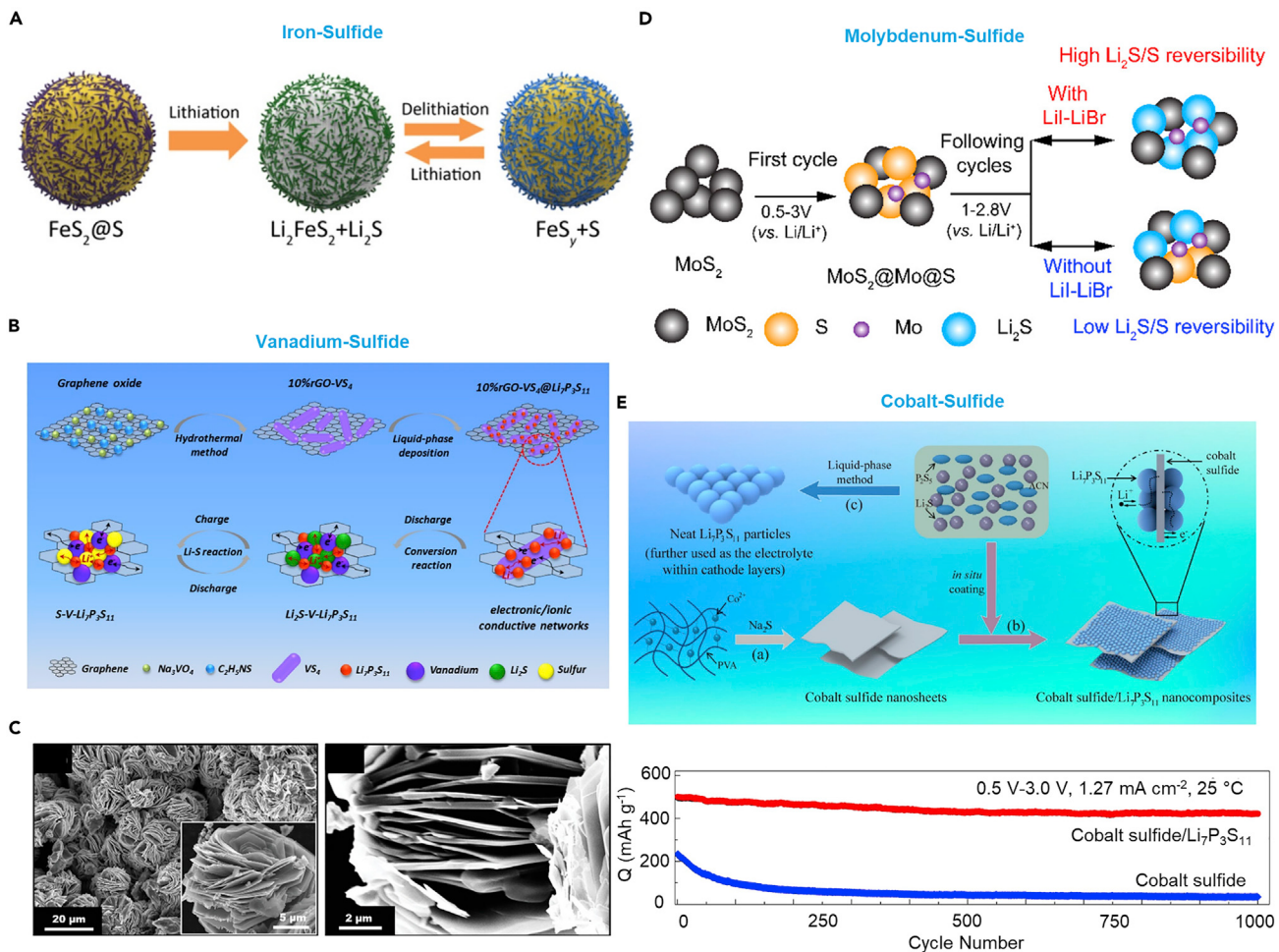
comprehensive overview of different cathode compositions/architectures and fabrication techniques that have been employed for SSLSB applications so far.

### MS<sub>x</sub>-based cathodes

Sulfur and its discharge products are ionically and electronically insulating species and thus require extra conducting additives for redox to occur efficiently. Because SSLSBs operate in the absence of a liquid electrolyte that can easily wet the electrodes, a significant fraction of SSE must be incorporated in the cathode composite to construct Li<sup>+</sup> ion-conducting pathways. Thus, a typical solid-state sulfur composite electrode consists of three components: (1) active material, (2) SSE, and (3) conductive carbon. A high contact area (so-called triphase interface) between the three components is essential for facilitating sulfur redox in the cathode composite. This presents an interesting dilemma because some of the best solid-state conductors, such as thiophosphates (e.g., Li<sub>10</sub>GeP<sub>2</sub>S<sub>12</sub> and Li<sub>3</sub>PS<sub>4</sub>) decompose when in close contact with electronically conductive conduits.<sup>75,76</sup> During decomposition, redox-active degradation products passivate the surface of the SSE. These degradation products are less conductive and impede charge transfer over the triphase interface, which severely compromises Coulombic efficiency in the initial cycles.<sup>77</sup> To address these challenges, various transition metal sulfides (e.g., MS<sub>2</sub> or MS, with M = Fe, V, Mo, Co, etc.) that exhibit high electronic and ionic conductivity as well as good chemical and interfacial stability with traditional thiophosphate SSEs have been used directly as active materials for SSLSB applications.

Ulissi et al.<sup>78</sup> demonstrated these principles by using carbon-iron disulfide-sulfur (C-FeS<sub>2</sub>-S)-based composites as an alternative cathode material, reporting an areal capacity of 3.55 mAh cm<sup>-2</sup> at a commercially relevant active material loading of 5 mg cm<sup>-2</sup> in SSLSB cells. However, these composites still have a relatively low Coulombic efficiency in the first cycle and can only maintain a stable capacity for less than 10 cycles, likely because of the relatively large amount of carbon additive (20 wt %), which induces SSE decomposition and poor interfacial contact between FeS<sub>2</sub> and S as a consequence of mixing via ball milling. To overcome these challenges, FeS<sub>2</sub>@S microspheres were fabricated using a simple liquid-phase method and used as the composite cathode material in SSLSBs (Figure 6A).<sup>79</sup> In this configuration, a thin layer of sulfur is embedded in a stable and conductive FeS<sub>2</sub> microsphere matrix. This clever engineering design alleviates the volume change and improves sulfur redox in the cathode layer, resulting in an excellent rate and cycling performance at room temperature. The enhanced performance can also be attributed to a smaller fraction of carbon additive (~10 wt %) in the composite, which minimizes SSE oxidation during charge.

Along with FeS<sub>2</sub>, linear-chain vanadium tetrasulfide (VS<sub>4</sub>) has also been investigated as an alternative positive electrode material for SSLSBs. For instance, Zhang et al.<sup>80</sup> synthesized reduced graphene oxide-VS<sub>4</sub> nanocomposites with *in situ*-coated SSE nanoparticles on the surface (10% reduced graphene oxide [rGO]-VS<sub>4</sub>@Li<sub>7</sub>P<sub>3</sub>S<sub>11</sub>) as a cathode composite material (Figure 6B). This combination of VS<sub>4</sub>, graphene, and Li<sub>7</sub>P<sub>3</sub>S<sub>11</sub> SSE enables multi-channel pathways that can facilitate charge transport in the cathode composite. When applied in an SSLSB configuration, the 10% rGO-VS<sub>4</sub>@Li<sub>7</sub>P<sub>3</sub>S<sub>11</sub> nanocomposites deliver a reversible capacity of 333 mAh g<sup>-1</sup> (based on sulfur content) for 500 cycles at a high current density of 0.5 A g<sup>-1</sup>. Then Xu et al.<sup>81</sup> reported an intercalation-conversion hybrid cathode using vanadium disulfide (VS<sub>2</sub>) nanoparticles with an exquisite flower-like structure (Figure 6C). Using a simple melt-diffusion method, sulfur is first coated onto VS<sub>2</sub> nanoparticles. After successful sulfur incorporation, the thiophosphate SSE β-Li<sub>3</sub>PS<sub>4</sub> is mixed with

**Figure 6. MS<sub>x</sub>-based cathodes for SSLSBs**

(A) Lithiation/delithiation process of FeS<sub>2</sub>@S microspheres. Reproduced with permission from Mwizerwa et al.<sup>79</sup> Copyright 2020, American Chemical Society.

(B) Synthesis process and reaction mechanism of 10% rGO-VS<sub>4</sub>@Li<sub>7</sub>P<sub>3</sub>S<sub>11</sub> nanocomposites. Reproduced with permission from Zhang et al.<sup>80</sup> Copyright 2019, Elsevier.

(C) Scanning electron microscopy (SEM) images of VS<sub>2</sub> nanoparticles with a flower-like structure. Reproduced with permission from Xu et al.<sup>81</sup> Copyright 2021, Wiley.

(D) Schematic showing the effect of the LiI-LiBr catalyst for MoS<sub>2</sub> cathodes. Reproduced with permission from Wan et al.<sup>82</sup> Copyright 2021, American Chemical Society.

(E) Fabrication method of cobalt sulfide-Li<sub>7</sub>P<sub>3</sub>S<sub>11</sub> nanocomposites and their corresponding cycling performance. Reproduced with permission from Yao et al.<sup>83</sup> Copyright 2016, American Chemical Society.

S@VS<sub>2</sub> to obtain S/VS<sub>2</sub>/β-Li<sub>3</sub>PS<sub>4</sub> composites. This two-step approach is critical because it maximizes the surface contact between sulfur and the electron conductor VS<sub>2</sub> while establishing an intermediate barrier between VS<sub>2</sub> and Li<sub>3</sub>PS<sub>4</sub>, which prevents SSE oxidation during charge. When applied in SSLSBs, the S/VS<sub>2</sub>/β-Li<sub>3</sub>PS<sub>4</sub> composite cathodes exhibit high sulfur utilization of approximately 85% and a Coulombic efficiency of 96% in the first cycle.

Transition metal sulfides are often challenged with the irreversible conversion between its lithiated and delithiated products. For instance, in the case of MoS<sub>2</sub>, its subsequent regeneration after lithiation is severely hindered by the poor redox kinetics of Li<sub>2</sub>S and S, which leads to rapid capacity decay and poor rate

**Table 2.** Literature review of MS<sub>x</sub>-based cathodes for SSLSBs

Cathode composite	Sulfur content (%)	Active material loading (mg cm <sup>-2</sup> )	SSE interlayer	Capacity after cycling (mAh g <sup>-1</sup> )	Cycle life	Current density	Temperature (°C)	Anode	Reference
C/FeS <sub>2</sub> -S/SSE (15–35–50)	15	1.0	Lil-LPS	1,200	20	83.5 mA g <sup>-1</sup>	20	Li	Ulissi et al. <sup>78</sup>
C/FeS <sub>2</sub> -S/SSE (15–35–50)	15	4.0	Lil-LPS	790	8	16.7 mA g <sup>-1</sup>	25	Li	Ulissi et al. <sup>78</sup>
C/FeS <sub>2</sub> -S/SSE (15–35–50)	15	5.0	Lil-LPS	710	7	16.7 mA g <sup>-1</sup>	25	Li	Ulissi et al. <sup>78</sup>
C/FeS <sub>2</sub> @S/SSE (10:40:50)	12	0.8	Li <sub>10</sub> GeP <sub>2</sub> S <sub>12</sub> /75% Li <sub>2</sub> S-24% P <sub>2</sub> S <sub>5</sub> -1% P <sub>2</sub> O <sub>5</sub>	430.7	200	30 mA g <sup>-1</sup>	25	Li	Mwizerwa et al. <sup>79</sup>
C/rGO-VS <sub>4</sub> @Li <sub>7</sub> P <sub>3</sub> S <sub>11</sub> /SSE (5:45:50)	N/A	0.9	Li <sub>10</sub> GeP <sub>2</sub> S <sub>12</sub> /75% Li <sub>2</sub> S-24% P <sub>2</sub> S <sub>5</sub> -1% P <sub>2</sub> O <sub>5</sub>	333	500	500 mA g <sup>-1</sup>	25	Li	Zhang et al. <sup>80</sup>
S-VS <sub>2</sub> /SSE (60:40)	2	1.0	β-LPS	N/A	10	0.12 mA g <sup>-1</sup>	25	Li	Xu et al. <sup>81</sup>
C/MoS <sub>2</sub> @Lil-LiBr@C/SSE (10:40:50)	N/A	N/A	Li <sub>10</sub> GeP <sub>2</sub> S <sub>12</sub> /75% Li <sub>2</sub> S-24% P <sub>2</sub> S <sub>5</sub> -1% P <sub>2</sub> O <sub>5</sub>	437.8	100	200 mA g <sup>-1</sup>	25	Li	Wan et al. <sup>82</sup>
C/Co <sub>x</sub> S <sub>y</sub> /SSE (10:40:50)	N/A	1.04	Li <sub>10</sub> GeP <sub>2</sub> S <sub>12</sub> /70% Li <sub>2</sub> S-29% P <sub>2</sub> S <sub>5</sub> -1% P <sub>2</sub> O <sub>5</sub>	421	1,000	1.27 mA g <sup>-1</sup>	25	Li	Yao et al. <sup>83</sup>

performance.<sup>84,85</sup> To tackle this issue, the catalytic compound Lil-LiBr was introduced into MoS<sub>2</sub> (MoS<sub>2</sub>@Lil-LiBr) to investigate its influence on sulfur redox in the cathode composite (Figure 6D).<sup>82</sup> It was found that Lil-LiBr considerably lowers the overpotential for Li<sub>2</sub>S delithiation, enabling good Li<sub>2</sub>S/S reversibility and improved reaction kinetics. When mixed with carbon black, the MoS<sub>2</sub>@Lil-LiBr@C cathodes can achieve a reversible capacity of 604.8 mAh g<sup>-1</sup> at 200 mA g<sup>-1</sup> for 100 cycles, demonstrating the effectiveness of catalytic incorporation in MS<sub>x</sub>-based cathodes for SSLSBs. In another approach, an *in situ* liquid-phase technique was used to fabricate cobalt sulfide nanosheets with Li<sub>7</sub>P<sub>3</sub>S<sub>11</sub> SSE nanoparticles (~10 nm) embedded on its surface (Figure 6E).<sup>83</sup> In this configuration, there is a high surface contact area between Li<sub>7</sub>P<sub>3</sub>S<sub>11</sub> and cobalt sulfide, which is beneficial for reducing the interfacial resistance between the two components. The cobalt sulfide-Li<sub>7</sub>P<sub>3</sub>S<sub>11</sub> nanocomposites achieve a reversible capacity of 421 mAh g<sup>-1</sup> at 1.27 mA cm<sup>-2</sup> after 1,000 cycles (Figure 6F), demonstrating their outstanding potential as alternative positive electrode materials. This approach contradicts some of the contributions presented above, which suggest that intimate contact between the SSE and electron source results in poor electrochemical performance by exacerbating SSE decomposition during charge. It can be inferred that a delicate balance should be achieved between the Li<sup>+</sup> and e<sup>-</sup> conductors in the cathode composite so that sulfur redox is maximized and SSE degradation is minimized. Identifying ways to strike a good balance between these components is a crucial step toward achieving high-performance SSLSBs that employ MS<sub>x</sub>-based cathodes. Table 2 provides a summary of recent articles that report MS<sub>x</sub>-based cathodes for SSLSBs.

### Li<sub>2</sub>S-based cathodes

Using Li<sub>2</sub>S as the initiating active material presents new opportunities because it can be coupled with a variety of anode materials apart from lithium, such as silicon, tin, and graphite.<sup>86–88</sup> Anode-free configurations can also be developed using Li<sub>2</sub>S, which considerably increases energy density.<sup>89–92</sup> A key issue with LSBs is the severe volume expansion/contraction of sulfur during (de)lithiation.<sup>93–95</sup> During this process, 1 mol of sulfur converts into 8 mols of Li<sub>2</sub>S, resulting in a volume expansion of approximately 80%. In a solid-state configuration, this results in formation of cracks and contact loss between the active materials and Li<sup>+</sup>/e<sup>-</sup> conducting channels in the cathode composite, resulting in fewer triphase interfaces and, thus, poor sulfur redox. Consequently, this volume-induced failure, also referred to as chemo-mechanical failure, considerably limits long-term cycling performance and often results in irreversible capacity.<sup>96,97</sup> A common approach that has been adopted to alleviate

chemo-mechanical failure is employing Li<sub>2</sub>S rather than sulfur as the active material. Li<sub>2</sub>S is in its least dense state (1.66 g cm<sup>-3</sup>) and, thus, can prevent electrode pulverization resulting from severe volume expansion during battery operation.<sup>98</sup> However, like its delithiated counterpart, Li<sub>2</sub>S suffers from poor electronic/ionic conductivity ( $1.0 \times 10^{-13}$  S cm<sup>-1</sup>, electronic conductivity) and exhibits a much higher activation potential.<sup>99</sup> Thus, establishing an intimate triphase interface between Li<sub>2</sub>S and the electronically/ionically conducting components in the cathode composite is even more necessary. In terms of its handling, Li<sub>2</sub>S is unstable under ambient environmental conditions and has low solubility in most organic solvents and a high melting temperature (938°C), making it difficult to adopt traditional cathode fabrication techniques when preparing S-based cathodes, such as melt-diffusion.<sup>100</sup>

Li<sub>2</sub>S-based cathodes have distinct advantages that can be leveraged to enable high-performance SSLSBs. Thus, many efforts have been made to fabricate Li<sub>2</sub>S-based cathodes. For instance, Han et al.<sup>101</sup> prepared a mixed-conductive Li<sub>2</sub>S nanocomposite using a coprecipitation/carbonization method (Figure 7A). First, Li<sub>2</sub>S, polyvinylpyrrolidone (PVP), and Li<sub>6</sub>PS<sub>5</sub>Cl are dissolved in ethanol and subsequently dried at 100°C to obtain Li<sub>2</sub>S-Li<sub>6</sub>PS<sub>5</sub>Cl-PVP nanocomposites. Upon heating at 550°C in an argon atmosphere, the PVP carbonizes and forms a carbon matrix, where Li<sub>2</sub>S and Li<sub>6</sub>PS<sub>5</sub>Cl nanoparticles (~4 nm in size) are uniformly distributed on its surface. The intimate surface contact between the three components enhances charge transfer kinetics in the cathode composite and lowers the activation energy of Li<sub>2</sub>S, enabling an active material utilization of 71% at a high Li<sub>2</sub>S loading of 3.6 mg cm<sup>-2</sup> at room temperature. This work demonstrates that a solution-based method can be used to effectively fabricate Li<sub>2</sub>S-based cathode composites. It shows that the high melting temperature of Li<sub>2</sub>S is a double-edged sword in the sense that it can be leveraged to enable high-temperature fabrication processes and new synthesis routes. In a similar approach, ultrasmall Li<sub>2</sub>S-CNT nanocomposites were prepared using a simple liquid-phase method (Figure 7B).<sup>102</sup> Here Li<sub>2</sub>S and CNTs are dissolved in anhydrous ethanol to obtain a homogenous solution. After thorough mixing, suction filtration is used to obtain a composite consisting of uniformly dispersed Li<sub>2</sub>S nanoparticles on a CNT substrate. This stable one-dimensional architecture considerably improves the electronic conductivity of Li<sub>2</sub>S while preventing its aggregation. When applied in an SSLSB configuration, the Li<sub>2</sub>S-CNT nanocomposites demonstrate excellent cycling stability, delivering a capacity of 651.4 mAh g<sup>-1</sup> for 300 cycles at a current density of 1 C. Yan et al.<sup>103</sup> fabricated a Li<sub>2</sub>S@C nanocomposite by combustion of lithium metal with carbon disulfide (CS<sub>2</sub>) (Figure 7C). During this combustion reaction, Li<sub>2</sub>S nanoparticles *in situ* form in a carbon matrix, establishing a percolated network of electronically/ionically conductive pathways when mixed with a Li<sub>7</sub>P<sub>3</sub>S<sub>11</sub> SSE. This unique architecture enables high Li<sub>2</sub>S utilization of 91% at high areal loading of 7 mg cm<sup>-2</sup> and delivers stable cycling for over 700 cycles.

The previous three contributions are examples of fabricating Li<sub>2</sub>S-based cathodes by depositing Li<sub>2</sub>S on different conductive substrates. The inverse has also been achieved. For instance, a liquid-phase shaking technique was used to prepare Li<sub>2</sub>S-Li<sub>3</sub>PS<sub>4</sub> composite materials with *in situ*-grown Li<sub>3</sub>PS<sub>4</sub> on the Li<sub>2</sub>S surface (Figure 7D).<sup>104</sup> This was done by first dissolving Li<sub>2</sub>S and P<sub>2</sub>S<sub>5</sub> in tetrahydrofuran. Upon heating at 320°C for 1 h, Li<sub>2</sub>S-Li<sub>3</sub>PS<sub>4</sub> composites with high ionic conductivity of  $1.11 \times 10^{-4}$  S cm<sup>-1</sup> are obtained. When mixed with carbon additives, the composite cathodes deliver a high specific capacity of 772.6 at 0.1 mA cm<sup>-2</sup> at a high active material loading of 50%. This work demonstrates the importance of establishing a high surface area contact between the active material and SSE to improve

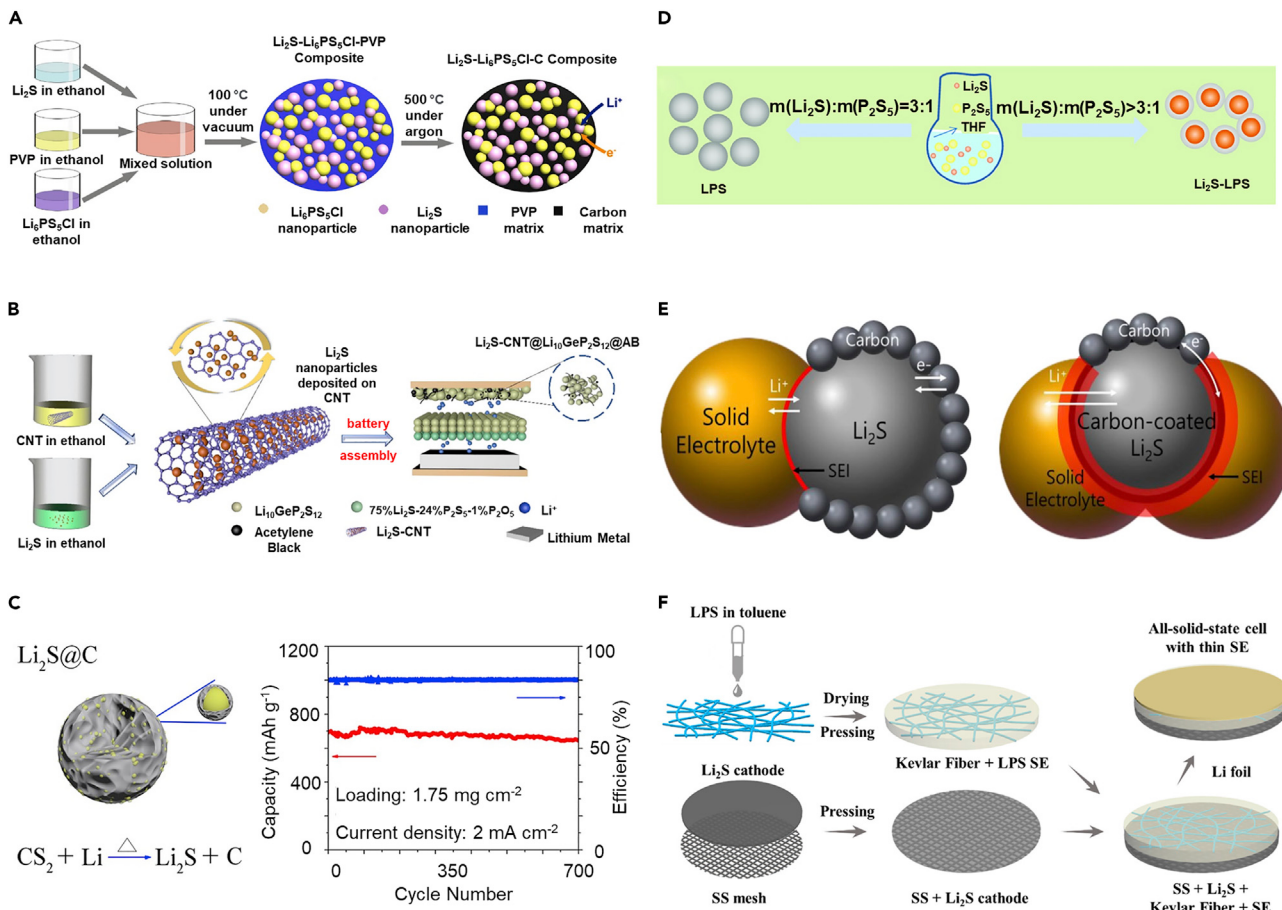


**Figure 7. Li<sub>2</sub>S-based cathodes for SSLSBs**

- (A) Coprecipitation/carbonization method for synthesizing mixed-conductive Li<sub>2</sub>S-Li<sub>6</sub>PS<sub>5</sub>Cl-PVP nanocomposites. Reproduced with permission from Han et al.<sup>101</sup> Copyright 2016, American Chemical Society.
- (B) Ultrasmall Li<sub>2</sub>S-CNT nanocomposites synthesized by a simple liquid-phase method using ethanol. Reproduced with permission from Jiang et al.<sup>102</sup> Copyright 2021, American Chemical Society.
- (C) Schematic of Li<sub>2</sub>S@C nanocomposites synthesized by combustion of lithium metal with CS<sub>2</sub> and their corresponding cycling performance. Reproduced with permission from Yan et al.<sup>103</sup> Copyright 2019, American Chemical Society.
- (D) Liquid-phase shaking technique used to prepare Li<sub>2</sub>S-LPS composite materials with *in situ*-grown LPS on the Li<sub>2</sub>S surface. Reproduced with permission from Jiang et al.<sup>104</sup> Copyright 2020, Wiley.
- (E) Schematic comparing lithium ion and electron transfer in bare Li<sub>2</sub>S and carbon-coated Li<sub>2</sub>S. Reproduced with permission from Choi et al.<sup>105</sup> Copyright 2018, Elsevier.
- (F) Schematic showing the fabrication process of a cathode-supported solid-state cell using a thin sulfide electrolyte. Reproduced with permission from Xu et al.<sup>106</sup> Copyright 2019, American Chemical Society.

charge transfer kinetics in the cathode composite. It presents an alternative liquid-phase shaking technique that can be used to fabricate Li<sub>2</sub>S-based cathodes. In a similar approach, carbon-coated Li<sub>2</sub>S cathodes were prepared by heating a solution containing PAN, 1-methyl-2-pyrrolidinone, and Li<sub>2</sub>S at 700°C for 5 h in an argon atmosphere (Figure 7E).<sup>105</sup> The carbon coating drastically increases the electronic conductivity of Li<sub>2</sub>S from  $9.21 \times 10^{-9}$  S cm<sup>-1</sup> to  $2.39 \times 10^{-2}$  S cm<sup>-1</sup>. Consequently, the total fraction of carbon additives in the cathode composite can be reduced, which is beneficial for maximizing the energy density of the cell. Unique cell designs have been used to enable thick Li<sub>2</sub>S cathodes with active material loading of up to 7.64 mg cm<sup>-2</sup>, correlating to an energy density of approximately 370.6 Wh kg<sup>-1</sup>.<sup>106</sup> In this approach, a cathode composite consisting of Li<sub>2</sub>S-LiI, vapor-grown

**Table 3.** Literature review of Li<sub>2</sub>S-based cathodes for SSLSBs

Cathode composite	Sulfur content (%)	Active material loading (mg cm <sup>-2</sup> )	SSE interlayer	Capacity after cycling (mAh g <sup>-1</sup> )	Cycle life	Current density	Temperature (°C)	Anode	Reference
C/Li <sub>2</sub> S-Li <sub>6</sub> PS <sub>5</sub> Cl-C/SSE (10:60:30)	36	3.6	80Li <sub>2</sub> S·20P <sub>2</sub> S <sub>5</sub>	830	60	0.18 mA cm <sup>-2</sup>	25	Li/In	Han et al. <sup>101</sup>
C/Li <sub>2</sub> S-CNT/SSE (20:30:50)	14	1.27	Li <sub>10</sub> GeP <sub>2</sub> S <sub>12</sub> /75% Li <sub>2</sub> S-24% P <sub>2</sub> S <sub>5</sub> -1% P <sub>2</sub> O <sub>5</sub>	651.4	300	2.12 mA cm <sup>-2</sup>	60	Li	Jiang et al. <sup>102</sup>
C/Li <sub>2</sub> S@C/SSE (10:30:30)	38	1.75	Li <sub>3</sub> P <sub>3</sub> S <sub>11</sub>	748	100	0.5 mA cm <sup>-2</sup>	25	Li/In	Yan et al. <sup>103</sup>
C/Li <sub>2</sub> S@C/SSE (10:30:30)	38	1.75	Li <sub>3</sub> P <sub>3</sub> S <sub>11</sub>	644	700	2.0 mA cm <sup>-2</sup>	60	Li/In	Yan et al. <sup>103</sup>
C/Li <sub>2</sub> S@C/SSE (10:30:30)	38	3.5	Li <sub>3</sub> P <sub>3</sub> S <sub>11</sub>	1,047	10	0.2 mA cm <sup>-2</sup>	25	Li/In	Yan et al. <sup>103</sup>
C/Li <sub>2</sub> S@C/SSE (10:30:30)	38	7.0	Li <sub>3</sub> P <sub>3</sub> S <sub>11</sub>	1,073	30	0.2 mA cm <sup>-2</sup>	60	Li/In	Yan et al. <sup>103</sup>
C/Li <sub>2</sub> S/SSE (20/36/44)	36	1.38	LPS	651	30	0.2 mA cm <sup>-2</sup>	60	Li/In	Jiang et al. <sup>104</sup>
C/Li <sub>2</sub> S-LPS (20/50/30)	50	1.92	LPS	674	30	0.2 mA cm <sup>-2</sup>	60	Li/In	Jiang et al. <sup>104</sup>
C/Li <sub>2</sub> S@C/SSE (6.25:31.25:62.5)	9	0.68	Li <sub>2</sub> S-P <sub>2</sub> S <sub>5</sub>	730	25	0.05 mA cm <sup>-2</sup>	25	Li/In	Choi et al. <sup>105</sup>
C/Li <sub>2</sub> S-Li/SSE (10:75:15)	43.4	2.54	LPS	636.4	50	0.21 mA cm <sup>-2</sup>	25	Li	Xu et al. <sup>106</sup>
C/Li <sub>2</sub> S-Li/SSE (10:75:15)	43.4	3.82	LPS	725	20	0.32 mA cm <sup>-2</sup>	25	Li	Xu et al. <sup>106</sup>
C/Li <sub>2</sub> S-Li/SSE (10:75:15)	43.4	5.10	LPS	600	20	0.43 mA cm <sup>-2</sup>	25	Li	Xu et al. <sup>106</sup>
C/Li <sub>2</sub> S-Li/SSE (10:75:15)	43.4	7.64	LPS	460	20	0.64 mA cm <sup>-2</sup>	25	Li	Xu et al. <sup>106</sup>

carbon fibers (VGCF), and Li<sub>3</sub>PS<sub>4</sub> (LPS) was first fabricated and subsequently cold pressed onto a stainless-steel mesh current collector (Figure 7F). The full cell was prepared by cold-pressing an LPS-Kevlar SSE on the cathode film and attaching a piece of lithium foil on top. The thin SSE layer enables employment of thick cathodes, which is crucial for maximizing energy density and enabling practical application of SSLSBs.

Significant progress has been made toward developing Li<sub>2</sub>S-based cathodes for SSLSB applications. Although using Li<sub>2</sub>S as the active material does not fully address all challenges associated with SSLSBs and even gives rise to other issues, such as high activation energy and moisture sensitivity, this approach provides new opportunities for SSLSB research and development. As mentioned previously, one of the biggest advantages of using Li<sub>2</sub>S over MS<sub>x</sub> or S is that it can be coupled with Li-free anode materials and enables anode-free configurations. Currently, work in these areas remains scarce but they are exciting avenues for more research. A summary of recent Li<sub>2</sub>S-based SSLSB reports is given in Table 3.

### S-based cathodes

Currently, the initiating active material that will be used for next-generation SSLSBs remains ambiguous. Sulfur-based cathodes are far superior to MS<sub>x</sub> and Li<sub>2</sub>S-based cathodes when considering cost.<sup>107,108</sup> Despite this, the practical energy density that can be achieved by sulfur-based cathodes in an SSLSB configuration is severely lacking. There is a dearth of studies that report SSLSB data using practical conditions, such as high sulfur loading and high areal capacity. However, endeavors to circumvent the fundamental challenges of SSLSBs that employ sulfur-based cathodes are hardly scarce.

It is widely known that, in the liquid state, the characteristics of the carbon additives have a major influence on the electrochemical behavior of LSBs by providing a conductive matrix that can increase active material utilization, prevent LiPS dissolution, and alleviate volume-induced failure during cycling.<sup>18,19,109</sup> The role of carbon additives in SSLSBs is also significant and has been demonstrated by recent studies. For instance, Sakuda et al.<sup>110</sup> prepared composite cathodes using mesoporous

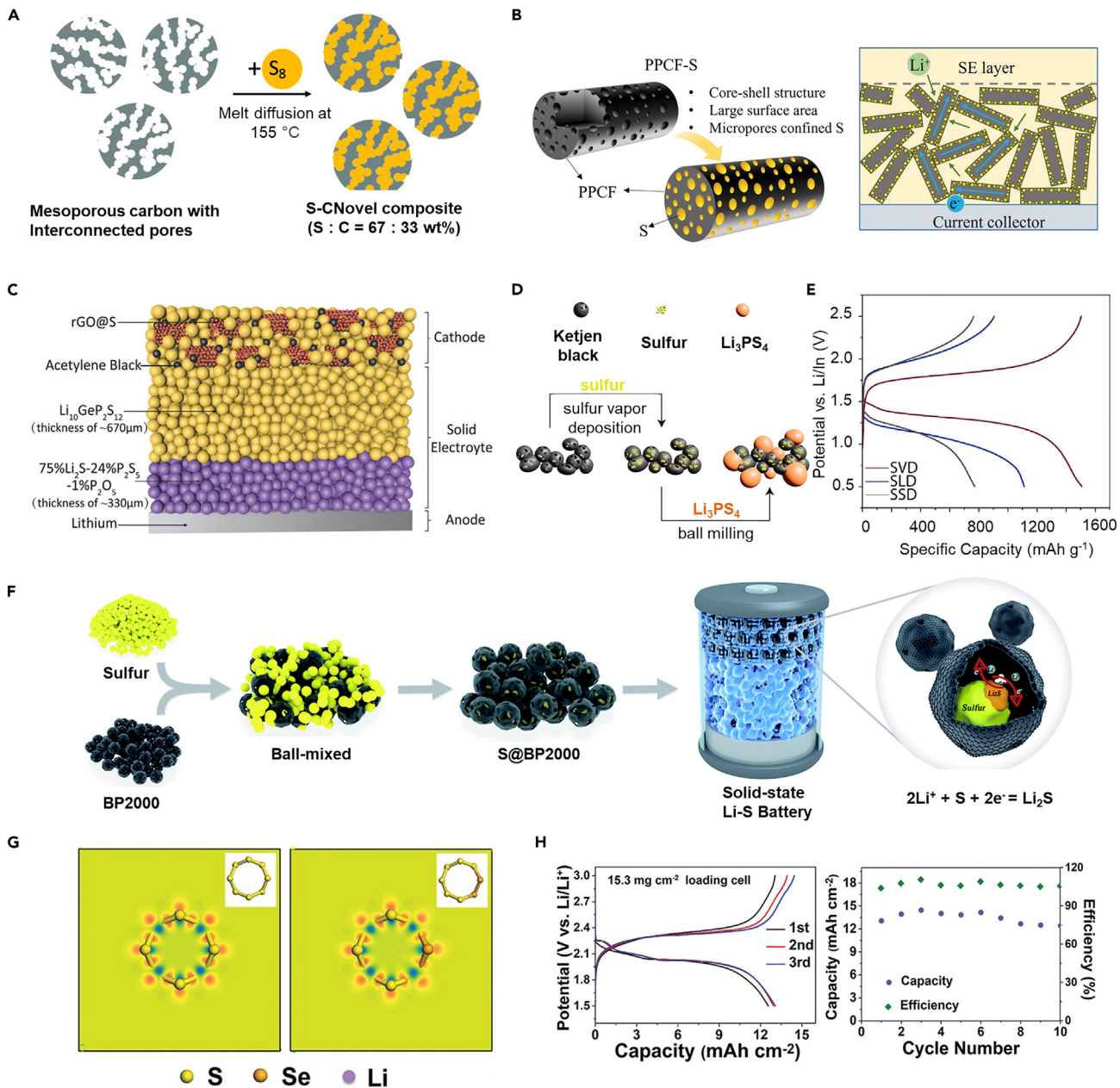


**Figure 8. S-based cathodes for SSLSBs**

(A) Oxide template method for fabricating composite cathodes using mesoporous carbon. Reproduced with permission from Sakuda et al.<sup>110</sup> Copyright 2019, Wiley.

(B) Schematic showing the morphology of PPCFs and the effect of using them as carbon additives in SSLSBs. Reproduced with permission from Sun et al.<sup>111</sup> Copyright 2022, Wiley.

(C) Schematic of SSLSB using the rGO@S cathode composite. Reproduced with permission from Yao et al.<sup>112</sup> Copyright 2017, Wiley.

(D) Synthesis of a three-component SSLSB cathode using the SVD method. Reproduced with permission from Alzahrani et al.<sup>113</sup> Copyright 2021, American Chemical Society.

(E) Charge/discharge profiles of SSLSB cathodes prepared using SVD, SLD, and SSD. Reproduced with permission from Alzahrani et al.<sup>113</sup> Copyright 2021, American Chemical Society.

(F) Schematic of the microporous S@BP2000 nanocomposite with core-shell morphology for SSLSBs. Reproduced with permission from Han et al.<sup>114</sup> Copyright 2019, Royal Society of Chemistry.

**Figure 8. Continued**

(G) DFT calculations for the bond breaking and lithiation reaction of the  $\text{Se}_2\text{S}_6$  ring and proposed intermediates, followed by the structure of  $\text{Se}_{2.57}\text{S}_{5.43}$  and Raman spectra for S, Se, and as-prepared  $\text{Se}_2\text{S}_6$ ,  $\text{SeS}_2$ ,  $\text{Se}_4\text{S}_4$ , and  $\text{Se}_6\text{S}_2$ . Reproduced with permission from Li et al.<sup>115</sup> Copyright 2019, Wiley.

(H) Schematic of the microporous S@BP2000 nanocomposite with core-shell morphology for SSLSBs. Reproduced with permission from Li et al.<sup>115</sup> Copyright 2019, Wiley.

carbon with interconnected pores fabricated by a simple oxide template method (Figure 8A). Compared with a traditional cathode composite using acetylene black, the as-prepared cathodes deliver a much higher reversible capacity ( $1,200 \text{ mAh g}^{-1}$  versus  $200 \text{ mAh g}^{-1}$ ) and can successfully operate at a high current density of  $5.2 \text{ mA cm}^{-2}$  at room temperature. In this work, the high mesoporous structure of the carbon material enables efficient conduction pathways that help facilitate sulfur redox during battery operation. In a similar approach, porous carbon fibers with core-shell morphology were fabricated by tuning the microstructure of PAN-derived carbon fibers (PPCFs) (Figure 8B).<sup>111</sup> The porous layer is present only at the surface of the carbon fibers, allowing semi-infiltration of sulfur upon melt-diffusion and effective contact between the  $\text{Li}^+$  and  $e^-$  conductors. This design is crucial because complete encapsulation of the sulfur particles impedes contact with the SSE, resulting in poor sulfur redox. Compared with traditional VGCFs, the PPCFs deliver a much higher initial capacity of  $1,166 \text{ mAh g}^{-1}$ , demonstrating the importance of structural design for SSLSBs cathodes. A sulfur-amine chemistry synthesis method has also been used to deposit amorphous sulfur nanoparticles (2 nm) onto an rGO substrate (rGO@S) (Figure 8C).<sup>112</sup> Here, the rGO layer acts as a conductive substrate and as a buffer for sulfur volume expansion. The uniform distribution of sulfur nanoparticles increases the contact area between the carbon and SSE in the composite, allowing efficient sulfur redox to occur. When tested in a full cell, the rGO@S cathodes maintain a stable capacity of  $830 \text{ mAh g}^{-1}$  for 750 cycles, demonstrating the importance of reducing the ion diffusion pathways and alleviating stress/strain in the cathode composite. Then Alzahrani et al.<sup>113</sup> revealed a new sulfur vapor deposition (SVD) approach for homogeneously depositing sulfur in a porous carbon matrix (Figure 8D). Sulfur is evaporated and then condensed so that it can effectively infiltrate the porous carbon matrix. When mixed with an LPS SSE and applied in a full cell, the SVD composite cathodes show enhanced rate performance, cycling stability, and high capacity compared with traditional fabrication routes, such as sulfur liquid deposition (SLD) and sulfur solid deposition (SSD) (Figure 8E). Recently, a microporous S@BP2000 nanocomposite with core-shell morphology fabricated using a simple melt-diffusion technique was demonstrated (Figure 8F).<sup>114</sup> In this design, the BP-2000 carbon can alleviate the insulating nature and volume expansion of sulfur because of its high surface area ( $1,739 \text{ m}^2 \text{ g}^{-1}$ ) and pore volume ( $2.747 \text{ cm}^3 \text{ g}^{-1}$ ). As a result, S@BP2000 nanocomposites deliver a high capacity of  $1,391.3 \text{ mAh g}^{-1}$  at  $0.2 \text{ C}$  while demonstrating an excellent cycling stability of over 1,200 cycles at  $3 \text{ C}$  with a capacity of  $985.3 \text{ mAh g}^{-1}$ . Active material utilization in S-based cathodes has also been enhanced by introducing selenium into the cathode composite in the form of  $\text{SeS}_x$  solid solutions.<sup>115</sup> Using density functional theory (DFT) calculations, the electron density distributions of an  $\text{S}_8$  ring and *ortho*- $\text{Se}_2\text{S}_6$  ring were compared (Figure 8G). It was found that the electronic conductivity of the  $\text{Se}_n\text{S}_{8-n}$  ring was greater than that of the pristine  $\text{S}_8$  ring because Se substitution induced more density states in the electronic structure of S atoms. Because the electronic conductivity of selenium is much higher than that of pure sulfur ( $1.0 \times 10^{-3}$  versus  $0.5 \times 10^{-27} \text{ S m}^{-1}$  at room temperature), it is expected that  $\text{Se}_n\text{S}_{8-n}$  cathodes can achieve superior electrochemical performance when applied as the cathode material in an SSLSB configuration.<sup>116–118</sup> To investigate the effect of Se introduction in SSLSBs, a high-loading  $\text{SeS}_2$ -based cathode of  $38.2 \text{ mg cm}^{-2}$  (corresponding to

**Table 4.** Literature review of S-based cathodes for SSLSBs

Cathode composite	Sulfur content (%)	Active material loading ( $\text{mg cm}^{-2}$ )	SSE interlayer	Capacity after cycling ( $\text{mAh g}^{-1}$ )	Cycle life	Current density	Temperature ( $^{\circ}\text{C}$ )	Anode	Reference
C/S/SSE (20:40:40)	40	2.6	LPS	1,100	400	$1.3 \text{ mA cm}^{-2}$	25	Li/In	Sakuda et al. <sup>110</sup>
C/S/SSE (10:40:50)	36	4.0	$\text{Li}_6\text{PS}_5\text{Cl}$	710	220	$0.67 \text{ mA cm}^{-2}$	25	Li/In	Sun et al. <sup>111</sup>
C/rGO@S/SSE (20:30:50)	12	0.5	$\text{Li}_{10}\text{GeP}_2\text{S}_{12}/75\%$ $\text{Li}_2\text{S}-24\% \text{P}_2\text{S}_5-1\%$ $\text{P}_2\text{O}_5$	830	750	$0.84 \text{ mA cm}^{-2}$	60	Li	Yao et al. <sup>112</sup>
C/S/SSE (15.4:38.5:46.1)	38.5	1.5	LPS	1,437	100	$0.25 \text{ mA cm}^{-2}$	60	Li/In	Alzahrani et al. <sup>113</sup>
C/S/SSE (15.4:38.5:46.1)	38.5	3.0	LPS	1250	50	$0.5 \text{ mA cm}^{-2}$	60	Li/In	Alzahrani et al. <sup>113</sup>
C/S/SSE (15.4:38.5:46.1)	38.5	4.5	LPS	950	50	$0.75 \text{ mA cm}^{-2}$	60	Li/In	Alzahrani et al. <sup>113</sup>
C/S/SSE (10:30:60)	30	0.45	$\text{Li}_7\text{P}_3\text{S}_{11}$	985.3	1,200	$2.26 \text{ mA cm}^{-2}$	25	Li/In	Han et al. <sup>114</sup>
C/S/SSE (10:30:60)	30	0.45	$\text{Li}_7\text{P}_3\text{S}_{11}$	1,221	500	$2.26 \text{ mA cm}^{-2}$	80	Li/In	Han et al. <sup>114</sup>
C/S/SSE (20:20:40)	25	1.3	$\text{Li}_{10}\text{GeP}_2\text{S}_{12}$	998.6	200	$0.21 \text{ mA cm}^{-2}$	N/A	Li/In	Hou et al. <sup>121</sup>
C/S/SSE (20:20:40)	25	3.8	$\text{Li}_{10}\text{GeP}_2\text{S}_{12}$	1,249.3	20	$0.13 \text{ mA cm}^{-2}$	N/A	Li/In	Hou et al. <sup>121</sup>
C/S/SSE (20:20:40)	25	5.9	$\text{Li}_{10}\text{GeP}_2\text{S}_{12}$	576.7	20	$0.1 \text{ mA cm}^{-2}$	N/A	Li/In	Hou et al. <sup>121</sup>
C/CNT@S/SSE (20:30:50)	26.6	0.5	$\text{Li}_{10}\text{GeP}_2\text{S}_{12}/75\%$ $\text{Li}_2\text{S}-24\% \text{P}_2\text{S}_5-1\%$ $\text{P}_2\text{O}_5$	660.3	400	$0.84 \text{ mA cm}^{-2}$	60	Li	Zhang et al. <sup>122</sup>
C/S@CNT/SSE (10:30:40)	26.3	1.07	$\text{Li}_{10}\text{GeP}_2\text{S}_{12}$	1,154	200	$0.36 \text{ mA cm}^{-2}$	N/A	Li/Al	Pan et al. <sup>123</sup>
C/S@C/SSE (20:50:30)	30	1.3	$\text{Li}_7\text{P}_3\text{S}_{11}$	881.3	100	$1.09 \text{ mA cm}^{-2}$	50	Li/In	Zhu et al. <sup>124</sup>
C/S/SSE (20:20:40)	25	1.1	$\text{Li}_6\text{PS}_5\text{Cl}$	1,066.8	100	$0.18 \text{ mA cm}^{-2}$	25	Li/In	Zhu et al. <sup>125</sup>
C/S/SSE (16:24:60)	24	1.06	$\text{Li}_6\text{PS}_5\text{Cl}$	1,393	50	$0.18 \text{ mA cm}^{-2}$	25	Li/In	Wang et al. <sup>126</sup>
C/S/SSE (15:25:60)	25	1.1	$\text{Li}_2\text{S}-\text{P}_2\text{S}_5$	834.3	1,000	$0.176 \text{ mA cm}^{-2}/$ $0.44 \text{ mA cm}^{-2}$	25	Li/In	Zhang et al. <sup>127</sup>

an  $\text{SeS}_2$  loading of  $15.3 \text{ mg cm}^{-2}$ ) was tested between 1.5 and 3.0 V at  $30 \text{ mA g}^{-1}$  and  $60^{\circ}\text{C}$  (Figure 8H). The high-loading cell is fully reversible and maintains an areal capacity of  $11.8 \text{ mAh cm}^{-2}$  at the 10th cycle (94% capacity retention). This work demonstrates that  $\text{SeS}_x$  solid solutions can enable SSLSBs with high active material utilization at ultra-high loading. In a similar approach, a tellurium-doped S@pPAN cathode was fabricated for SSLSBs. The reactivity and cycling stability of the SSLSBs improve with introduction of tellurium because of its high electronic conductivity and excellent compatibility with the SSE.<sup>119</sup> Our group demonstrated a halide-based solid-state lithium-selenium battery (SSLSB), showing excellent compatibility between Se (or  $\text{Li}_x\text{Se}_y$ ) species with the halide SSE.<sup>120</sup> Whether halide SSEs have similar compatibility with sulfur species and can be used in the SSLSB system is unclear but worthy of investigation.

Sulfur cathodes face many challenges that are intrinsic to the sulfur material itself, such as low conductivity and large volume expansion. Thus, effective use of sulfur as the initiating active material in SSLSBs heavily depends on cathode composite design and engineering, particularly regarding the carbon additives, as demonstrated by previous studies. Future work should investigate new cathode composite configurations that can enable high active material utilization under high sulfur loading conditions while minimizing the amount of carbon additives. Table 4 summarizes recent SSLSB reports using S-based cathodes to guide future work.

A solid-state configuration is an assured way to eliminate the shuttle effect phenomenon and enable SfLSBs. Although the cathode composite materials do not play any role in promoting a solid-solid conversion pathway like in the liquid state, the significance of the initiating active material, whether that is  $\text{MS}_x$ ,  $\text{Li}_2\text{S}$ , or S, cannot be understated. Each material presents its own unique opportunities and challenges that can be leveraged to enable high-performance SSLSBs for next-generation applications and devices.

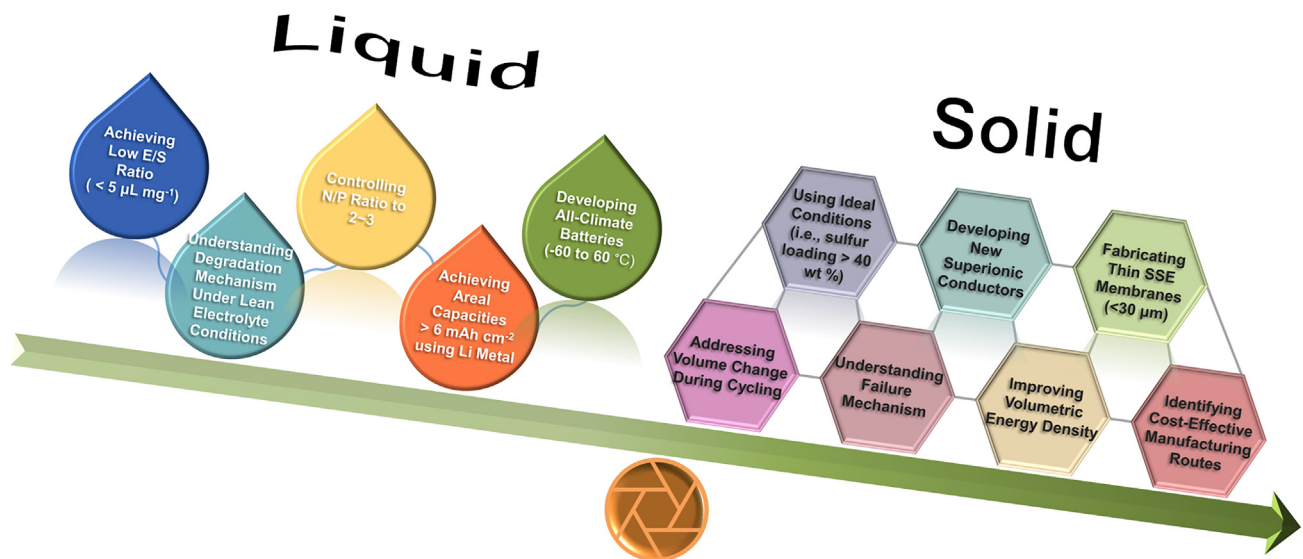


**Figure 9.** Future perspectives for liquid/solid-state SfLSBs

## CONCLUSION AND PERSPECTIVES

In this review, we provide a fundamental understanding of SfLSBs by comparing their operating mechanism with traditional LSBs. Then various strategies that have been used to enable liquid-state SfLSBs are presented, placing emphasis on cathode composite materials based on S-PAN composites, sulfur molecule confinement, chemical stabilization via metal/non-metal doping, and others. A transition is made toward describing all-SSSLBs, highlighting the design and fabrication of cathode composites depending on the initiating active material, such as transition metal-sulfides, lithium-sulfide, and sulfur. SfLSBs are a promising energy storage system with vast potential to enable the commercial application of LSBs. However, SfLSBs are not without challenges, and the timeline for their fruition remains obscure. Here we present key challenges that impede SfSB technology and provide a comprehensive guideline that serves to assist academic and industrial researchers in their future endeavors regarding this highly promising system (Figure 9).

### Liquid SfLSB perspectives

#### Achieving a low E/S ratio

The critical bottleneck for LSB commercialization stems from the difficulty to realize practical energy density at the pouch cell level. In this regard, a low E/S ratio ( $< 3 \mu\text{L mg}^{-1}$ ) is critical for achieving LSBs that can compete with the current state of the art.<sup>128</sup> Dense/thick electrodes and functional binders that can enable a lower E/S ratio without compromising electrochemical performance should be developed.<sup>129</sup> This will help increase the energy density of LSBs, which is critical for next-generation applications such as EVs.

#### Elucidating the degradation mechanism via advanced characterization

Systematic studies that utilize theoretical calculations and advanced characterization techniques, such as NMR and DFT, and synchrotron-based techniques, like *in situ* X-ray absorption (XAS) or XANES should be leveraged to elucidate the dynamic diffusion behavior and the degradation mechanism of LSBs, especially under lean electrolyte conditions.<sup>130–132</sup> This will enable a better fundamental understanding regarding the working mechanism of practical LSB configurations.

### Controlling the N/P ratio

Concerns stemming from dendrite-induced failure at the anode side during cycling has severely compromised the areal capacity of LSB cells. Future work should look to improve the areal capacity of lithium anodes to  $\sim 4\text{--}6 \text{ mAh cm}^{-2}$  without sacrificing safety and cycling stability.<sup>128</sup> A stabilized lithium metal anode will ensure enhanced Coulombic efficiency, which, in turn, improves long-term cycling. The ultimate goal in terms of maximizing the energy density coming from the anode side would be to employ thin lithium metal.<sup>133</sup> In other words, controlling the N/P ratio to  $\sim 2\text{--}3$  is crucial for realizing practical LSBs.

### Developing all-climate LSBs

All-climate LSBs that can effectively operate in a temperature range of  $-60$  to  $60^\circ\text{C}$  while possessing excellent electrochemical performance should be developed because this is a crucial prerequisite for many applications, such as EVs.

### Solid S<sub>f</sub>LSB perspectives

#### Demonstrating SSLSBs using ideal conditions

Currently, SSLSBs can only achieve satisfactory electrochemical performance under ideal laboratory conditions, such as at low sulfur content (<30%) and low areal capacity (<1.5  $\text{mAh cm}^{-2}$ ). Under such conditions, SSLSBs lose one of their strongest merits: high energy density. For SSLSBs to become a commercial success, future contributions should look to (1) increase the sulfur loading in the cathode composite to above 50%, (2) improve the areal capacity of sulfur cathodes to  $\sim 4\text{--}6 \text{ mAh cm}^{-2}$ , (3) employ high-energy-density lithium metal anodes<sup>128</sup>, (4) decrease the anode-to-cathode ratio to at least  $\sim 2\text{--}3$ , and (5) achieve working batteries for a wide range of temperatures (i.e.,  $-60^\circ\text{C}$  to  $60^\circ\text{C}$ ). These criteria must be satisfied to realize SSLSBs with high energy density, especially at the pouch cell level.

#### Developing new superionic conductors

Because SSLSBs operate in the absence of a liquid electrolyte that can easily wet the cathode, a fraction of SSE must be added to the cathode composite simply to achieve enough ionic percolation for  $\text{Li}^+$  transport. In this regard, the microstructure or "architecture" of cathode composites in a solid-state configuration is critical for guaranteeing non-tortuous conduction pathways and effective ionic conductivity that can facilitate sulfur redox. Although many SSEs, such as the thiophosphates  $\text{Li}_{10}\text{GeP}_2\text{S}_{12}$  and  $\text{Li}_6\text{PS}_5\text{Cl}$ , exhibit high ionic conductivity in the bulk, their conductivity is severely compromised when composited with other material, such as sulfur and carbon. Many SSEs, especially thiophosphates, have a limited electrochemical stability window ( $\sim 1.7\text{--}2.1 \text{ V vs. Li}^+/\text{Li}$ ). Thus, a large interfacial contact between the SSE and electron-conductive additives induces decomposition, leading to poor sulfur redox. This calls for development of new superionic conductors that possess ultra-high conductivity and excellent voltage stability.<sup>134–137</sup> These two thrusts are critical for achieving practical SSLSBs with high mass loading and active material utilization.

#### Fabricating thin SSE membranes

Although oxide-based SSEs are unsuitable as the  $\text{Li}^+$  conductor in the cathode composite because of their relatively lower conductivity in comparison with many thiophosphates, the ionic conductivity of the SSE interlayer can be lower than the SSE that is used in the cathode composite. In other words, if the SSE interlayer is thin, then the ionic conductivity does not need to be so high (i.e., above 10  $\text{mS cm}^{-1}$ ). Developing methods that can fabricate thin SSE membranes (<30  $\mu\text{m}$ ) without sacrificing their conductive, mechanical, and thermal properties is critical

for maximizing the energy density of SSLSBs and realizing their commercial application.<sup>129,138–140</sup>

#### *Addressing volume change during cycling*

Some promising directions to address the volume change of S-based cathodes in SSLSBs include (1) incorporating polymeric binders in the cathode composite. This calls for development of highly conductive, ductile, and chemically stable binders that can effectively suppress the volume change of sulfur without impeding charge transfer and applying thin-film coatings using atomic/molecular layer deposition (ALD/MLD) to alleviate volume change and address the insulating nature of sulfur.<sup>141–143</sup> The development of coatings that can be deposited at temperatures below the melting point of sulfur (<155°C) is crucial for ensuring effective deposition. High-temperature ALD/MLD coatings may be used for Li<sub>2</sub>S-based cathodes to improve the insulating nature of Li<sub>2</sub>S. However, the relatively low conductivity of common coatings, such as oxides and fluorides, will impede charge transfer at the triphase interface. Thus, ALD/MLD coatings with high conductivity and ductility should be explored. Applying external pressure (~1–3 tons) is a common approach to alleviate chemo-mechanical failure during cycling. However, this is impractical, especially at the pouch cell level, because external systems required to keep cells under constant pressure increases the volume, weight, and cost of the entire battery pack, sacrificing overall energy density. Future work should look to eliminate this pressure reliance through careful material and engineering design.

#### *Understanding failure mechanism*

Currently, the failure mechanism of SSLSBs remains ambiguous. In this regard, gaining a fundamental understanding of the triphase interface that forms between sulfur, carbon, and SSE is critical. Systematic studies that employ *in situ* characterization techniques, such as XAS, NMR, Raman spectroscopy, and XRD are vital for understanding the complex interfacial chemistry of SSLSBs.<sup>144–146</sup> High-throughput machine learning can also be used to gain a better understanding of the failure mechanism of SSLSBs.<sup>147</sup> However, this approach is still nascent.

#### *Improving volumetric energy density*

In the solid and liquid state, efforts to enhance the volumetric energy density (Wv) have been scarce, with many studies focusing on improving the gravimetric energy density (Wg) and cycling performance. Without achieving a high Wv of above 700 Wh L<sup>-1</sup>, LSB technology becomes increasingly moot, especially for next-generation applications, such as electric planes and aerial drones, that must obtain energy in a confined space.<sup>51,148</sup> Future work should pay equal attention to Wg and Wv. Some ways to improve the Wv of LSBs includes (1) maximizing the sulfur content of the cathode composite, (2) developing fabrication methods that can construct compact electrodes, and (3) using active materials with higher density, such as metal sulfides.

#### *Identifying cost-effective manufacturing routes*

Although SSLSB technology is still nascent, it is important to look at the long term and recognize challenges beyond fundamental research. Identifying cost-effective manufacturing routes that can easily utilize pre-existing infrastructure established at battery giga-factories around the world is crucial for realizing industrial adoption of SSLSBs.<sup>149,150</sup> Identifying and developing binders and solvents that are compatible with SSB materials is crucial for industrial success of SSLSBs.

## ACKNOWLEDGMENTS

This work was supported by the Natural Sciences and Engineering Research Council of Canada (NSERC), the Canada Research Chair Program (CRC), the Canada Foundation for Innovation (CFI), the Ontario Research Foundation (ORF), and the University of Western Ontario. J.T.K. thanks Prof. Y.Z. for fruitful discussions. C.W. acknowledges financial support from the Banting Postdoctoral Fellowship (BPF – 180162).

## AUTHOR CONTRIBUTIONS

Conceptualization, C.W. and J.T.K.; writing – original draft, J.T.K. and X.H.; writing – review & editing, J.T.K., X.H., C.W., and X.S.; supervision, X.S.

## DECLARATION OF INTERESTS

The authors declare no competing interests.

## REFERENCES

- Østergaard, P.A., Duic, N., Noorollahi, Y., Mikulcic, H., and Kalogirou, S. (2020). Sustainable development using renewable energy technology. *Renew. Energy* 146, 2430–2437. <https://doi.org/10.1016/j.renene.2019.08.094>.
- Deng, J., Bae, C., Denlinger, A., and Miller, T. (2020). Electric vehicles batteries: requirements and challenges. *Joule* 4, 511–515. <https://doi.org/10.1016/j.joule.2020.01.013>.
- Choi, J.W., and Aurbach, D. (2016). Promise and reality of post-lithium-ion batteries with high energy densities. *Nat. Rev. Mater.* 1, 16013. <https://doi.org/10.1038/natrevmats.2016.13>.
- Abada, S., Marlair, G., Lecocq, A., Petit, M., Sauvant-Moynot, V., and Huet, F. (2016). Safety focused modeling of lithium-ion batteries: a review. *J. Power Sources* 306, 178–192. <https://doi.org/10.1016/J.JPOWSOUR.2015.11.100>.
- Chen, Y., Kang, Y., Zhao, Y., Wang, L., Liu, J., Li, Y., Liang, Z., He, X., Li, X., Tavajohi, N., and Li, B. (2021). A review of lithium-ion battery safety concerns: the issues, strategies, and testing standards. *J. Energy Chem.* 59, 83–99. <https://doi.org/10.1016/J.JECHEM.2020.10.017>.
- Turcheniuk, K., Bondarev, D., Amatucci, G.G., and Yushin, G. (2021). Battery materials for low-cost electric transportation. *Mater. Today* 42, 57–72. <https://doi.org/10.1016/j.mattod.2020.09.027>.
- Yang, Y., Okonkwo, E.G., Huang, G., Xu, S., Sun, W., and He, Y. (2021). On the sustainability of lithium ion battery industry – a review and perspective. *Energy Storage Mater.* 36, 186–212. <https://doi.org/10.1016/J.ENSIM.2020.12.019>.
- Winslow, K.M., Laux, S.J., and Townsend, T.G. (2018). A review on the growing concern and potential management strategies of waste lithium-ion batteries. *Resour. Conserv. Recycl.* 129, 263–277. <https://doi.org/10.1016/J.RESCONREC.2017.11.001>.
- Yin, Y.-X., Xin, S., Guo, Y.-G., and Wan, L.-J. (2013). Lithium-sulfur batteries: electrochemistry, materials, and prospects. *Angew. Chem. Int. Ed. Engl.* 52, 13186–13200. <https://doi.org/10.1002/anie.201304762>.
- Zhang, S.S. (2013). Liquid electrolyte lithium-sulfur battery: fundamental chemistry, problems, and solutions. *J. Power Sources* 231, 153–162. <https://doi.org/10.1016/J.JPOWSOUR.2012.12.102>.
- Rosenman, A., Markevich, E., Salitra, G., Aurbach, D., Garsuch, A., and Chesneau, F.F. (2015). Review on Li-sulfur battery systems: an integral perspective. *Adv. Energy Mater.* 5, 1500212. <https://doi.org/10.1002/aenm.201500212>.
- Zhou, D., and Wang, G. (2020). Supercool sulfur. *Nat. Nanotechnol.* 15, 167–168. <https://doi.org/10.1038/s41565-019-0625-5>.
- Manthiram, A., Fu, Y., Chung, S.-H., Zu, C., and Su, Y.-S. (2014). Rechargeable lithium-sulfur batteries. *Chem. Rev.* 114, 11751–11787. <https://doi.org/10.1021/cr500062v>.
- Diao, Y., Xie, K., Xiong, S., and Hong, X. (2013). Shuttle phenomenon – the irreversible oxidation mechanism of sulfur active material in Li-S battery. *J. Power Sources* 235, 181–186. <https://doi.org/10.1016/j.jpowsour.2013.01.132>.
- Cheng, X.-B., Huang, J.-Q., Zhang, Q., Peng, H.-J., Zhao, M.-Q., and Wei, F. (2014). Aligned carbon nanotube/sulfur composite cathodes with high sulfur content for lithium-sulfur batteries. *Nano Energy* 4, 65–72. <https://doi.org/10.1016/j.nanoen.2013.12.013>.
- Zhang, C., Wu, H.B., Yuan, C., Guo, Z., and Lou, X.W. (2012). Confining sulfur in double-shelled hollow carbon spheres for lithium-sulfur batteries. *Angew. Chem. Int. Ed. Engl.* 51, 9592–9595. <https://doi.org/10.1002/anie.201205292>.
- Wang, H., Yang, Y., Liang, Y., Robinson, J.T., Li, Y., Jackson, A., Cui, Y., and Dai, H. (2011). Graphene-wrapped sulfur particles as a rechargeable lithium-sulfur battery cathode material with high capacity and cycling stability. *Nano Lett.* 11, 2644–2647. <https://doi.org/10.1021/nl200658a>.
- Xu, Z.-L., Kim, J.-K., and Kang, K. (2018). Carbon nanomaterials for advanced lithium sulfur batteries. *Nano Today* 19, 84–107. <https://doi.org/10.1016/j.nantod.2018.02.006>.
- Borchardt, L., Oschatz, M., and Kaskel, S. (2016). Carbon materials for lithium sulfur batteries—ten critical questions. *Chemistry* 22, 7324–7351. <https://doi.org/10.1002/chem.201600040>.
- Yang, X., Gao, X., Sun, Q., Jand, S.P., Yu, Y., Zhao, Y., Li, X., Adair, K., Kuo, L.Y., Rohrer, J., et al. (2019). Promoting the transformation of  $\text{Li}_2\text{S}_2$  to  $\text{Li}_2\text{S}$ : significantly increasing utilization of active materials for high-sulfur-loading Li-S batteries. *Adv. Mater.* 31, 1901220. <https://doi.org/10.1002/adma.201901220>.
- Du, Z., Chen, X., Hu, W., Chuang, C., Xie, S., Hu, A., Yan, W., Kong, X., Wu, X., Ji, H., and Wan, L.J. (2019). Cobalt in nitrogen-doped graphene as single-atom catalyst for high-sulfur content lithium-sulfur batteries. *J. Am. Chem. Soc.* 141, 3977–3985. <https://doi.org/10.1021/jacs.8b12973>.
- Xu, Z.-L., Lin, S., Onofrio, N., Zhou, L., Shi, F., Lu, W., Kang, K., Zhang, Q., and Lau, S.P. (2018). Exceptional catalytic effects of black phosphorus quantum dots in shuttling-free lithium sulfur batteries. *Nat. Commun.* 9, 4164. <https://doi.org/10.1038/s41467-018-0629-9>.
- Hao, X., Ma, J., Cheng, X., Zhong, G., Yang, J.L., Huang, L., Ling, H., Lai, C., Lv, W., Kang, F., et al. (2021). Electron and ion Co-conductive catalyst achieving instant transformation of lithium polysulfide towards  $\text{Li}_2\text{S}$ . *Adv. Mater.* 33, 2105362. <https://doi.org/10.1002/adma.202105362>.
- Chen, Y., Gao, X., Su, D., Wang, C., and Wang, G. (2020). Accelerating redox kinetics of lithium-sulfur batteries. *Trends Chem.* 2, 1020–1033. <https://doi.org/10.1016/j.trechm.2020.09.001>.

25. Li, X., Yuan, L., Liu, D., Xiang, J., Li, Z., and Huang, Y. (2022). Solid/quasi-solid phase conversion of sulfur in lithium–sulfur battery. *Small*, 2106970. <https://doi.org/10.1002/smll.202106970>.
26. Bhargav, A., He, J., Gupta, A., and Manthiram, A. (2020). Lithium–sulfur batteries: attaining the critical metrics. *Joule* 4, 285–291. <https://doi.org/10.1016/j.joule.2020.01.001>.
27. Zhang, Y., Zhang, X., Silva, S.R.P., Ding, B., Zhang, P., and Shao, G. (2022). Lithium–sulfur batteries meet electrospinning: recent advances and the key parameters for high gravimetric and volume energy density. *Adv. Sci.* 9, 2103879. <https://doi.org/10.1002/advs.202103879>.
28. Xing, C., Chen, H., Qian, S., Wu, Z., Nizami, A., Li, X., Zhang, S., and Lai, C. (2022). Regulating liquid and solid-state electrolytes for solid-phase conversion in Li–S batteries. *Chem* 8, 1201–1230. <https://doi.org/10.1016/j.chempr.2022.01.002>.
29. Ren, W., Ma, W., Zhang, S., and Tang, B. (2019). Recent advances in shuttle effect inhibition for lithium sulfur batteries. *Energy Storage Mater.* 23, 707–732. <https://doi.org/10.1016/j.ensm.2019.02.022>.
30. Zhang, S., Ueno, K., Dokko, K., and Watanabe, M. (2015). Recent advances in electrolytes for lithium–sulfur batteries. *Adv. Energy Mater.* 5, 1500117. <https://doi.org/10.1002/aenm.201500117>.
31. Zhang, S.S. (2013). Sulfurized carbon: a class of cathode materials for high performance lithium/sulfur batteries. *Front. Energy Res.* 1. <https://doi.org/10.3389/fenrg.2013.00010>.
32. Zhao, X., Wang, C., Li, Z., Hu, X., Abdul Razzaq, A., and Deng, Z. (2021). Sulfurized polyacrylonitrile for high-performance lithium sulfur batteries: advances and prospects. *J. Mater. Chem.* 9, 19282–19297. <https://doi.org/10.1039/D1TA03300J>.
33. Wang, W., Cao, Z., Elia, G.A., Wu, Y., Wahyudi, W., Abou-Hamad, E., Emwas, A.-H., Cavallo, L., Li, L.-J., and Ming, J. (2018). Recognizing the mechanism of sulfurized polyacrylonitrile cathode materials for Li–S batteries and beyond in Al–S batteries. *ACS Energy Lett.* 3, 2899–2907. <https://doi.org/10.1021/acsenergylett.8b01945>.
34. Wang, J., Yang, J., Xie, J., and Xu, N. (2002). A novel conductive polymer-sulfur composite cathode material for rechargeable lithium batteries. *Adv. Mater.* 14, 963–965. [https://doi.org/10.1002/1521-4095\(20020705\)14:13<963::AID-ADMA963>3.0.CO;2-1](https://doi.org/10.1002/1521-4095(20020705)14:13<963::AID-ADMA963>3.0.CO;2-1).
35. Yu, X.g., Xie, J.y., Yang, J., Huang, H.j., Wang, K., and Wen, Z.s. (2004). Lithium storage in conductive sulfur-containing polymers. *J. Electroanal. Chem.* 573, 121–128. <https://doi.org/10.1016/j.jelechem.2004.07.004>.
36. Yang, H., Chen, J., Yang, J., and Wang, J. (2020). Prospect of sulfurized pyrolyzed poly(acrylonitrile) (S@pPAN) cathode materials for rechargeable lithium batteries. *Angew. Chem. Int. Ed. Engl.* 59, 7306–7318. <https://doi.org/10.1002/anie.201913540>.
37. Yang, H., Naveed, A., Li, Q., Guo, C., Chen, J., Lei, J., Yang, J., Nuli, Y., and Wang, J. (2018). Lithium sulfur batteries with compatible electrolyte both for stable cathode and dendrite-free anode. *Energy Storage Mater.* 15, 299–307. <https://doi.org/10.1016/j.ensm.2018.05.014>.
38. He, B., Rao, Z., Cheng, Z., Liu, D., He, D., Chen, J., Miao, Z., Yuan, L., Li, Z., and Huang, Y. (2021). Rationally design a sulfur cathode with solid-phase conversion mechanism for high cycle-stable Li–S batteries. *Adv. Energy Mater.* 11, 2003690. <https://doi.org/10.1002/aenm.202003690>.
39. Li, H., Xue, W., Wang, L., and Liu, T. (2021). Two competing reactions of sulfurized polyacrylonitrile produce high-performance lithium–sulfur batteries. *ACS Appl. Mater. Interfaces* 13, 25002–25009. <https://doi.org/10.1021/acsami.1c06004>.
40. Abdul Razzaq, A., Yuan, X., Chen, Y., Hu, J., Mu, Q., Ma, Y., Zhao, X., Miao, L., Ahn, J.-H., Peng, Y., and Deng, Z. (2020). Anchoring MOF-derived CoS<sub>2</sub> on sulfurized polyacrylonitrile nanofibers for high areal capacity lithium–sulfur batteries. *J. Mater. Chem.* 8, 1298–1306. <https://doi.org/10.1039/C9TA11390H>.
41. Weret, M.A., Kuo, C.-F.J., Su, W.-N., Zeleke, T.S., Huang, C.-J., Sahalie, N.A., Zegeye, T.A., Wondimkun, Z.T., Fenta, F.W., Jote, B.A., et al. (2022). Fibrous organosulfur cathode materials with high bonded sulfur for high-performance lithium–sulfur batteries. *J. Power Sources* 541, 231693. <https://doi.org/10.1016/j.jpowsour.2022.231693>.
42. Yin, L., Wang, J., Lin, F., Yang, J., and Nuli, Y. (2012). Polyacrylonitrile/graphene composite as a precursor to a sulfur-based cathode material for high-rate rechargeable Li–S batteries. *Energy Environ. Sci.* 5, 6966. <https://doi.org/10.1039/c2ee03495f>.
43. Wang, X., Qian, Y., Wang, L., Yang, H., Li, H., Zhao, Y., and Liu, T. (2019). Sulfurized polyacrylonitrile cathodes with high compatibility in both ether and carbonate electrolytes for ultrastable lithium–sulfur batteries. *Adv. Funct. Mater.* 29, 1902929. <https://doi.org/10.1002/adfm.201902929>.
44. Wang, K., Zhao, T., Zhang, N., Feng, T., Li, L., Wu, F., and Chen, R. (2021). Powering lithium–sulfur batteries by ultrathin sulfurized polyacrylonitrile nanosheets. *Nanoscale* 13, 16690–16695. <https://doi.org/10.1039/D1NR04825B>.
45. Wang, L., He, X., Li, J., Chen, M., Gao, J., and Jiang, C. (2012). Charge/discharge characteristics of sulfurized polyacrylonitrile composite with different sulfur content in carbonate based electrolyte for lithium batteries. *Electrochim. Acta* 72, 114–119. <https://doi.org/10.1016/j.electacta.2012.04.005>.
46. Chen, H., Wang, C., Hu, C., Zhang, J., Gao, S., Lu, W., and Chen, L. (2015). Vulcanization accelerator enabled sulfurized carbon materials for high capacity and high stability of lithium–sulfur batteries. *J. Mater. Chem.* 3, 1392–1395. <https://doi.org/10.1039/C4TA05938G>.
47. Chen, W.J., Li, B.Q., Zhao, C.X., Zhao, M., Yuan, T.Q., Sun, R.C., Huang, J.Q., and Zhang, Q. (2020). Electrolyte regulation towards stable lithium–metal anodes in lithium–sulfur batteries with sulfurized polyacrylonitrile cathodes. *Angew. Chem. Int. Ed. Engl.* 59, 10732–10745. <https://doi.org/10.1002/anie.201912701>.
48. Zhou, G., Chen, H., and Cui, Y. (2022). Formulating energy density for designing practical lithium–sulfur batteries. *Nat. Energy* 7, 312–319. <https://doi.org/10.1038/s41560-022-01001-0>.
49. Chen, Z.X., Zhao, M., Hou, L.P., Zhang, X.Q., Li, B.Q., and Huang, J.Q. (2022). Toward practical high-energy-density lithium–sulfur pouch cells: a review. *Adv. Mater.* 34, e2201555. <https://doi.org/10.1002/adma.202201555>.
50. Chen, Y., Wang, T., Tian, H., Su, D., Zhang, Q., and Wang, G. (2021). Advances in lithium–sulfur batteries: from academic research to commercial viability. *Adv. Mater.* 33, 2003666. <https://doi.org/10.1002/adma.202003666>.
51. Xue, W., Miao, L., Qie, L., Wang, C., Li, S., Wang, J., and Li, J. (2017). Gravimetric and volumetric energy densities of lithium–sulfur batteries. *Curr. Opin. Electrochem.* 6, 92–99. <https://doi.org/10.1016/j.coelec.2017.10.007>.
52. Zhang, J., Li, Z., and Lou, X.W.D. (2017). A freestanding selenium disulfide cathode based on cobalt disulfide-decorated multichannel carbon fibers with enhanced lithium storage performance. *Angew. Chem. Int. Ed. Engl.* 56, 14107–14112. <https://doi.org/10.1002/anie.201708105>.
53. Xu, G.-L., Ma, T., Sun, C.-J., Luo, C., Cheng, L., Ren, Y., Heald, S.M., Wang, C., Curtiss, L., Wen, J., et al. (2016). Insight into the capacity fading mechanism of amorphous Se<sub>2</sub>S<sub>5</sub> confined in micro/mesoporous carbon matrix in ether-based electrolytes. *Nano Lett.* 16, 2663–2673. <https://doi.org/10.1021/acs.nanolett.6b00318>.
54. Li, Z., Zhang, J., Wu, H.B., and Lou, X.W.D. (2017). An improved Li–SeS<sub>2</sub> battery with high energy density and long cycle life. *Adv. Energy Mater.* 7, 1700281. <https://doi.org/10.1002/aenm.201700281>.
55. Xin, S., Gu, L., Zhao, N.H., Yin, Y.X., Zhou, L.J., Guo, Y.G., and Wan, L.J. (2012). Smaller sulfur molecules promise better lithium/sulfur batteries. *J. Am. Chem. Soc.* 134, 18510–18513. <https://doi.org/10.1021/ja308170k>.
56. Li, Z., Yuan, L., Yi, Z., Sun, Y., Liu, Y., Jiang, Y., Shen, Y., Xin, Y., Zhang, Z., and Huang, Y. (2014). Insight into the electrode mechanism in lithium–sulfur batteries with ordered microporous carbon confined sulfur as the cathode. *Adv. Energy Mater.* 4, 1301473. <https://doi.org/10.1002/aenm.201301473>.
57. Helen, M., Diemant, T., Schindler, S., Behm, R.J., Danzer, M., Kaiser, U., Fichtner, M., and Anji Reddy, M. (2018). Insight into sulfur confined in ultramicroporous carbon. *ACS Omega* 3, 11290–11299. <https://doi.org/10.1021/acsomega.8b01681>.
58. Zheng, S., Yi, F., Li, Z., Zhu, Y., Xu, Y., Luo, C., Yang, J., and Wang, C. (2014). Copper-stabilized sulfur-microporous carbon cathodes for Li–S batteries. *Adv. Funct. Mater.* 24, 4156–4163. <https://doi.org/10.1002/adfm.201304156>.

59. Sun, F., Zhang, B., Tang, H., Yue, Z., Li, X., Yin, C., and Zhou, L. (2018). Heteroatomic Te<sub>x</sub>S<sub>1-x</sub> molecule/C nanocomposites as stable cathode materials in carbonate-based electrolytes for lithium–chalcogen batteries. *J. Mater. Chem. 6*, 10104–10110. <https://doi.org/10.1039/C8TA02751J>.
60. Li, X., Liang, J., Zhang, K., Hou, Z., Zhang, W., Zhu, Y., and Qian, Y. (2015). Amorphous S-rich S<sub>1-x</sub>Sex/C ( $x \leq 0.1$ ) composites promise better lithium-sulfur batteries in a carbonate-based electrolyte. *Energy Environ. Sci.* 8, 3181–3186. <https://doi.org/10.1039/c5ee01470k>.
61. Yao, Y., Zeng, L., Hu, S., Jiang, Y., Yuan, B., and Yu, Y. (2017). Binding S<sub>0.6</sub>Se<sub>0.4</sub> in 1D carbon nanofiber with CS bonding for high-performance flexible Li-S batteries and Na-S batteries. *Small* 13, 1603513. <https://doi.org/10.1002/smll.201603513>.
62. Zeng, L., Yao, Y., Shi, J., Jiang, Y., Li, W., Gu, L., and Yu, Y. (2016). A flexible S<sub>1-x</sub>Sex@porous carbon nanofibers ( $x \leq 0.1$ ) thin film with high performance for Li-S batteries and room-temperature Na-S batteries. *Energy Storage Mater.* 5, 50–57. <https://doi.org/10.1016/j.ensm.2016.05.011>.
63. Zhang, X., Hu, G., Chen, K., Shen, L., Xiao, R., Tang, P., Yan, C., Cheng, H.-M., Sun, Z., and Li, F. (2022). Structure-related electrochemical behavior of sulfur-rich polymer cathode with solid-solid conversion in lithium-sulfur batteries. *Energy Storage Mater.* 45, 1144–1152. <https://doi.org/10.1016/j.ensm.2021.11.014>.
64. Chen, X., Yuan, L., Li, Z., Chen, S., Ji, H., Qin, Y., Wu, L., Shen, Y., Wang, L., Hu, J., and Huang, Y. (2019). Realizing an applicable “solid → solid” cathode process via a transplantable solid electrolyte interface for lithium–sulfur batteries. *ACS Appl. Mater. Interfaces* 11, 29830–29837. <https://doi.org/10.1021/acsami.9b07787>.
65. Li, X., Lushington, A., Sun, Q., Xiao, W., Liu, J., Wang, B., Ye, Y., Nie, K., Hu, Y., Xiao, Q., et al. (2016). Safe and durable high-temperature lithium-sulfur batteries via molecular layer deposited coating. *Nano Lett.* 16, 3545–3549. <https://doi.org/10.1021/acs.nanolett.6b00577>.
66. Li, X., Banis, M., Lushington, A., Yang, X., Sun, Q., Zhao, Y., Liu, C., Li, Q., Wang, B., Xiao, W., et al. (2018). A high-energy sulfur cathode in carbonate electrolyte by eliminating polysulfides via solid-phase lithium-sulfur transformation. *Nat. Commun.* 9, 4509. <https://doi.org/10.1038/s41467-018-06877-9>.
67. Tian, Y., Zeng, G., Rutt, A., Shi, T., Kim, H., Wang, J., Koettgen, J., Sun, Y., Ouyang, B., Chen, T., et al. (2021). Promises and challenges of next-generation “beyond Li-ion” batteries for electric vehicles and grid decarbonization. *Chem. Rev.* 121, 1623–1669. <https://doi.org/10.1021/acs.chemrev.0c00767>.
68. Sun, Y.-K. (2020). Promising all-solid-state batteries for future electric vehicles. *ACS Energy Lett.* 5, 3221–3223. <https://doi.org/10.1021/acsenergylett.0c01977>.
69. Zheng, F., Kotobuki, M., Song, S., Lai, M.O., and Lu, L. (2018). Review on solid electrolytes for all-solid-state lithium-ion batteries. *J. Power Sources* 389, 198–213. <https://doi.org/10.1016/J.JPOWSOUR.2018.04.022>.
70. Kim, J.G., Son, B., Mukherjee, S., Schuppert, N., Bates, A., Kwon, O., Choi, M.J., Chung, H.Y., and Park, S. (2015). A review of lithium and non-lithium based solid state batteries. *J. Power Sources* 282, 299–322. <https://doi.org/10.1016/J.JPOWSOUR.2015.02.054>.
71. Yang, X., Luo, J., and Sun, X. (2020). Towards high-performance solid-state Li-S batteries: from fundamental understanding to engineering design. *Chem. Soc. Rev.* 49, 2140–2195. <https://doi.org/10.1039/c9cs00635d>.
72. Hassoun, J., and Scrosati, B. (2010). Moving to a solid-state configuration: a valid approach to making lithium-sulfur batteries viable for practical applications. *Adv. Mater.* 22, 5198–5201. <https://doi.org/10.1002/adma.201002584>.
73. Lei, D., Shi, K., Ye, H., Wan, Z., Wang, Y., Shen, L., Li, B., Yang, Q.H., Kang, F., and He, Y.B. (2018). Progress and perspective of solid-state lithium-sulfur batteries. *Adv. Funct. Mater.* 28, 1707570. <https://doi.org/10.1002/adfm.201707570>.
74. Pan, H., Cheng, Z., He, P., and Zhou, H. (2020). A review of solid-state lithium-sulfur battery: ion transport and polysulfide chemistry. *Energy Fuels* 34, 11942–11961. <https://doi.org/10.1021/acs.energyfuels.0c02647>.
75. Koerver, R., Walther, F., Aygün, I., Sann, J., Dietrich, C., Zeier, W.G., and Janek, J. (2017). Redox-active cathode interphases in solid-state batteries. *J. Mater. Chem. 5*, 22750–22760. <https://doi.org/10.1039/C7TA07641J>.
76. Zhang, W., Richter, F.H., Culver, S.P., Leichtweiss, T., Lozano, J.G., Dietrich, C., Bruce, P.G., Zeier, W.G., and Janek, J. (2018). Degradation mechanisms at the Li<sub>10</sub>GeP<sub>2</sub>S<sub>12</sub>/LiCoO<sub>2</sub> cathode interface in an all-solid-state lithium-ion battery. *ACS Appl. Mater. Interfaces* 10, 22226–22236. <https://doi.org/10.1021/acsami.8b05132>.
77. Ohno, S., and Zeier, W.G. (2021). Toward practical solid-state Lithium–Sulfur batteries: challenges and perspectives. *Acc. Mater. Res.* 2, 869–880. <https://doi.org/10.1021/accountsmr.1c00116>.
78. Ulissi, U., Ito, S., Hosseini, S.M., Varzi, A., Aihara, Y., and Passerini, S. (2018). High capacity all-solid-state lithium batteries enabled by pyrite-sulfur composites. *Adv. Energy Mater.* 8, 1801462. <https://doi.org/10.1002/aenm.201801462>.
79. Mwizerwa, J.P., Zhang, Q., Han, F., Wan, H., Cai, L., Wang, C., and Yao, X. (2020). Sulfur-embedded FeS<sub>2</sub> as a high-performance cathode for room temperature all-solid-state lithium-sulfur batteries. *ACS Appl. Mater. Interfaces* 12, 18519–18525. <https://doi.org/10.1021/acsami.0c01607>.
80. Zhang, Q., Wan, H., Liu, G., Ding, Z., Mwizerwa, J.P., and Yao, X. (2019). Rational design of multi-channel continuous electronic/ionic conductive networks for room temperature vanadium tetrasulfide-based all-solid-state lithium-sulfur batteries. *Nano Energy* 57, 771–782. <https://doi.org/10.1016/j.nanoen.2019.01.004>.
81. Xu, S., Kwok, C.Y., Zhou, L., Zhang, Z., Kochetkov, I., and Nazar, L.F. (2021). A high capacity all solid-state Li-sulfur battery enabled by conversion-intercalation hybrid cathode architecture. *Adv. Funct. Mater.* 31, 2004239. <https://doi.org/10.1002/adfm.202004239>.
82. Wan, H., Zhang, B., Liu, S., Zhang, J., Yao, X., and Wang, C. (2021). Understanding Li<sub>1</sub>LiBr catalyst activity for solid state Li<sub>2</sub>S/S reactions in an all-solid-state lithium battery. *Nano Lett.* 21, 8488–8494. <https://doi.org/10.1021/acs.nanolett.1c03415>.
83. Yao, X., Liu, D., Wang, C., Long, P., Peng, G., Hu, Y.-S., Li, H., Chen, L., and Xu, X. (2016). High-energy all-solid-state lithium batteries with ultralong cycle life. *Nano Lett.* 16, 7148–7154. <https://doi.org/10.1021/acs.nanolett.6b03448>.
84. Stephenson, T., Li, Z., Olsen, B., and Mitlin, D. (2014). Lithium ion battery applications of molybdenum disulfide (MoS<sub>2</sub>) nanocomposites. *Energy Environ. Sci.* 7, 209–231. <https://doi.org/10.1039/C3EE42591F>.
85. Li, X., Zai, J., Xiang, S., Liu, Y., He, X., Xu, Z., Wang, K., Ma, Z., and Qian, X. (2016). Regeneration of metal sulfides in the delithiation process: the key to cyclic stability. *Adv. Energy Mater.* 6, 1601056. <https://doi.org/10.1002/aenm.201601056>.
86. Agostini, M., Hassoun, J., Liu, J., Jeong, M., Nara, H., Momma, T., Osaka, T., Sun, Y.-K., and Scrosati, B. (2014). A lithium-ion sulfur battery based on a carbon-coated lithium-sulfide cathode and an electrodeposited silicon-based anode. *ACS Appl. Mater. Interfaces* 6, 10924–10928. <https://doi.org/10.1021/am4057166>.
87. Hassoun, J., and Scrosati, B. (2010). A high-performance polymer tin sulfur lithium ion battery. *Angew. Chem.* 122, 2421–2424. <https://doi.org/10.1002/ange.200907324>.
88. Fu, Y., Zu, C., and Manthiram, A. (2013). In situ -formed Li<sub>2</sub>S in lithiated graphite electrodes for lithium–sulfur batteries. *J. Am. Chem. Soc.* 135, 18044–18047. <https://doi.org/10.1021/ja409705u>.
89. He, J., Bhargav, A., and Manthiram, A. (2022). High-performance anode-free Li–S batteries with an integrated Li<sub>2</sub>S–Electrocatalyst cathode. *ACS Energy Lett.* 7, 583–590. <https://doi.org/10.1021/acsenergylett.1d02569>.
90. Chen, J., Xiang, J., Chen, X., Yuan, L., Li, Z., and Huang, Y. (2020). Li<sub>2</sub>S-based anode-free full batteries with modified Cu current collector. *Energy Storage Mater.* 30, 179–186. <https://doi.org/10.1016/J.ESNM.2020.05.009>.
91. Nanda, S., Gupta, A., and Manthiram, A. (2018). A lithium-sulfur cell based on reversible lithium deposition from a Li<sub>2</sub>S cathode host onto a hostless-anode substrate. *Adv. Energy Mater.* 8, 1801556. <https://doi.org/10.1002/aenm.201801556>.
92. Ren, Y., Bhargav, A., Shin, W., Sul, H., and Manthiram, A. (2022). Anode-free lithium-sulfur cells enabled by rationally tuning lithium polysulfide molecules. *Angew. Chem.*

- Int. Ed. Engl. 61, e202207907. <https://doi.org/10.1002/anie.202207907>.
93. Wei Seh, Z., Li, W., Cha, J.J., Zheng, G., Yang, Y., McDowell, M.T., Hsu, P.-C., and Cui, Y. (2013). Sulphur–TiO<sub>2</sub> yolk–shell nanoarchitecture with internal void space for long-cycle lithium–sulphur batteries. Nat. Commun. 4, 1331. <https://doi.org/10.1038/ncomms2327>.
  94. Shaibani, M., Mirshekarloo, M.S., Singh, R., Easton, C.D., Cooray, M.C.D., Eshraghi, N., Abendroth, T., Dörfler, S., Althues, H., Kaskel, S., et al. (2020). Expansion-tolerant architectures for stable cycling of ultrahigh-loading sulfur cathodes in lithium-sulfur batteries. Sci. Adv. 6, eaay2757. <https://doi.org/10.1126/sciadv.aay2757>.
  95. Waluś, S., Offer, G., Hunt, I., Patel, Y., Stockley, T., Williams, J., and Purkayastha, R. (2018). Volumetric expansion of Lithium-Sulfur cell during operation – fundamental insight into applicable characteristics. Energy Storage Mater. 10, 233–245. <https://doi.org/10.1016/j.ensm.2017.05.017>.
  96. Koerver, R., Zhang, W., de Biasi, L., Schweidler, S., Kondrakov, A.O., Kolling, S., Brezesinski, T., Hartmann, P., Zeier, W.G., and Janek, J. (2018). Chemo-mechanical expansion of lithium electrode materials – on the route to mechanically optimized all-solid-state batteries. Energy Environ. Sci. 11, 2142–2158. <https://doi.org/10.1039/C8EE00907D>.
  97. Oh, Y.S., Kim, M., Kang, S., Park, J.Y., and Lim, H.T. (2022). Redox activity of Li<sub>2</sub>S–P2S5 electrolyte inducing chemo-mechanical failure in all-solid-state batteries comprising sulfur composite cathode and Li–Si alloy anode. Chem. Eng. J. 442, 136229. <https://doi.org/10.1016/J.CEJ.2022.136229>.
  98. Kaiser, M.R., Han, Z., Liang, J., Dou, S.-X., and Wang, J. (2019). Lithium sulfide-based cathode for lithium-ion/sulfur battery: recent progress and challenges. Energy Storage Mater. 19, 1–15. <https://doi.org/10.1016/j.ensm.2019.04.001>.
  99. Ye, H., Li, M., Liu, T., Li, Y., and Lu, J. (2020). Activating Li<sub>2</sub>S as the lithium-containing cathode in lithium–sulfur batteries. ACS Energy Lett. 5, 2234–2245. <https://doi.org/10.1021/acsenergylett.0c00936>.
  100. Lee, S.-K., Lee, Y.J., and Sun, Y.-K. (2016). Nanostructured lithium sulfide materials for lithium-sulfur batteries. J. Power Sources 323, 174–188. <https://doi.org/10.1016/j.jpowsour.2016.05.037>.
  101. Han, F., Yue, J., Fan, X., Gao, T., Luo, C., Ma, Z., Suo, L., and Wang, C. (2016). High-performance all-solid-state lithium–sulfur battery enabled by a mixed-conductive Li<sub>2</sub>S nanocomposite. Nano Lett. 16, 4521–4527. <https://doi.org/10.1021/acs.nanolett.6b01754>.
  102. Jiang, M., Liu, G., Zhang, Q., Zhou, D., and Yao, X. (2021). Ultrasmall Li<sub>2</sub>S-carbon nanotube nanocomposites for high-rate all-solid-state lithium–sulfur batteries. ACS Appl. Mater. Interfaces 13, 18666–18672. <https://doi.org/10.1021/acsami.1c00511>.
  103. Yan, H., Wang, H., Wang, D., Li, X., Gong, Z., and Yang, Y. (2019). In situ generated Li<sub>2</sub>S–C nanocomposite for high-capacity and long-life all-solid-state lithium sulfur batteries with ultrahigh areal mass loading. Nano Lett. 19, 3280–3287. <https://doi.org/10.1021/acs.nanolett.9b00882>.
  104. Jiang, H., Han, Y., Wang, H., Zhu, Y., Guo, Q., Jiang, H., Zheng, C., and Xie, K. (2020). Li<sub>2</sub>S–Li<sub>3</sub>PS<sub>4</sub> (LPS) composite synthesized by liquid-phase shaking for all-solid-state lithium–sulfur batteries with high performance. Energy Technol. 8, 2000023. <https://doi.org/10.1002/ente.202000023>.
  105. Choi, S., Yoon, I., Nichols, W.T., and Shin, D. (2018). Carbon-coated Li<sub>2</sub>S cathode for improving the electrochemical properties of an all-solid-state lithium-sulfur battery using Li<sub>2</sub>S–P2S5 solid electrolyte. Ceram. Int. 44, 7450–7453. <https://doi.org/10.1016/j.ceramint.2018.01.104>.
  106. Xu, R., Yue, J., Liu, S., Tu, J., Han, F., Liu, P., and Wang, C. (2019). Cathode-supported all-solid-state lithium–sulfur batteries with high cell-level energy density. ACS Energy Lett. 4, 1073–1079. <https://doi.org/10.1021/acsenergylett.9b00430>.
  107. Yin, Y.-X., Xin, S., Guo, Y.-G., and Wan, L.-J. (2013). Lithium-sulfur batteries lithium-sulfur batteries: electrochemistry, materials, and prospects. Angew. Chem. Int. Ed. Engl. 52, 13186–13200. <https://doi.org/10.1002/anie.201304762>.
  108. Li, G., Chen, Z., and Lu, J. (2018). Lithium–sulfur batteries for commercial applications. Chem. 4, 3–7. <https://doi.org/10.1016/J.CHEMPR.2017.12.012>.
  109. Li, Z., Huang, Y., Yuan, L., Hao, Z., and Huang, Y. (2015). Status and prospects in sulfur–carbon composites as cathode materials for rechargeable lithium–sulfur batteries. Carbon 92, 41–63. <https://doi.org/10.1016/j.carbon.2015.03.008>.
  110. Sakuda, A., Sato, Y., Hayashi, A., and Tatsumisago, M. (2019). Sulfur-based composite electrode with interconnected mesoporous carbon for all-solid-state lithium–sulfur batteries. Energy Technol. 7, 1900077. <https://doi.org/10.1002/ente.201900077>.
  111. Sun, X., Li, Q., Cao, D., Wang, Y., Anderson, A., and Zhu, H. (2022). High surface area N-doped carbon fibers with accessible reaction sites for all-solid-state lithium-sulfur batteries. Small 18, 2105678. <https://doi.org/10.1002/smll.202105678>.
  112. Yao, X., Huang, N., Han, F., Zhang, Q., Wan, H., Mwizerwa, J.P., Wang, C., and Xu, X. (2017). High-performance all-solid-state lithium–sulfur batteries enabled by amorphous sulfur-coated reduced graphene oxide cathodes. Adv. Energy Mater. 7, 1602923. <https://doi.org/10.1002/aenm.201602923>.
  113. Alzahrani, A.S., Otaki, M., Wang, D., Gao, Y., Arthur, T.S., Liu, S., and Wang, D. (2021). Confining sulfur in porous carbon by vapor deposition to achieve high-performance cathode for all-solid-state lithium–sulfur batteries. ACS Energy Lett. 6, 413–418. <https://doi.org/10.1021/acsenergylett.0c01956>.
  114. Han, Q., Li, X., Shi, X., Zhang, H., Song, D., Ding, F., and Zhang, L. (2019). Outstanding cycle stability and rate capabilities of the all-solid-state Li–S battery with a Li<sub>7</sub>P<sub>3</sub>S<sub>11</sub> glass-ceramic electrolyte and a core–shell S@BP2000 nanocomposite. J. Mater. Chem. 7, 3895–3902. <https://doi.org/10.1039/C8TA12443D>.
  115. Li, X., Liang, J., Luo, J., Wang, C., Li, X., Sun, Q., Li, R., Zhang, L., Yang, R., Lu, S., et al. (2019). High-performance Li–SeS x all-solid-state lithium batteries. Adv. Mater. 31, e1808100. <https://doi.org/10.1002/adma.201808100>.
  116. Zhang, F., Guo, X., Xiong, P., Zhang, J., Song, J., Yan, K., Gao, X., Liu, H., and Wang, G. (2020). Interface engineering of MXene composite separator for high-performance Li–Se and Na–Se batteries. Adv. Energy Mater. 10, 2000446. <https://doi.org/10.1002/aenm.202000446>.
  117. Li, J., Song, J., Luo, L., Zhang, H., Feng, J., Zhao, X., Guo, X., Dong, H., Chen, S., Liu, H., et al. (2022). Synergy of MXene with Se infiltrated porous N-doped carbon nanofibers as janus electrodes for high-performance sodium/lithium–selenium batteries. Adv. Energy Mater. 12, 2200894. <https://doi.org/10.1002/aenm.202200894>.
  118. Tian, H., Tian, H., Wang, S., Chen, S., Zhang, F., Song, L., Liu, H., Liu, J., and Wang, G. (2020). High-power lithium–selenium batteries enabled by atomic cobalt electrocatalyst in hollow carbon cathode. Nat. Commun. 11, 5025. <https://doi.org/10.1038/s41467-020-18820-y>.
  119. Zhang, W., Zhang, Y., Peng, L., Li, S., Wang, X., Cheng, S., and Xie, J. (2020). Elevating reactivity and cyclability of all-solid-state lithium–sulfur batteries by the combination of tellurium-doping and surface coating. Nano Energy 76, 105083. <https://doi.org/10.1016/j.nanoen.2020.105083>.
  120. Li, X., Liang, J., Kim, J.T., Fu, J., Duan, H., Chen, N., et al. (2022). Highly Stable Halide-Electrolyte-Based All-Solid-State Li–Se Batteries (Advanced Materials), 2200856.
  121. Hou, L.-P., Yuan, H., Zhao, C.-Z., Xu, L., Zhu, G.-L., Nan, H.-X., Cheng, X.-B., Liu, Q.-B., He, C.-X., Huang, J.-Q., and Zhang, Q. (2020). Improved interfacial electronic contacts powering high sulfur utilization in all-solid-state lithium–sulfur batteries. Energy Storage Mater. 25, 436–442. <https://doi.org/10.1016/j.ensm.2019.09.037>.
  122. Zhang, Q., Huang, N., Huang, Z., Cai, L., Wu, J., and Yao, X. (2020). CNTs@S composite as cathode for all-solid-state lithium–sulfur batteries with ultralong cycle life. J. Energy Chem. 40, 151–155. <https://doi.org/10.1016/j.jechem.2019.03.006>.
  123. Pan, H., Zhang, M., Cheng, Z., Jiang, H., Yang, J., Wang, P., He, P., and Zhou, H. (2022). Carbon-free and binder-free Li–Al alloy anode enabling an all-solid-state Li–S battery with high energy and stability. Sci. Adv. 8, eabn4372. <https://doi.org/10.1126/sciadv.eabn4372>.
  124. Zhu, X., Jiang, W., Zhao, S., Huang, R., Ling, M., Liang, C., and Wang, L. (2022). Exploring the concordant solid-state electrolytes for

- all-solid-state lithium-sulfur batteries. *Nano Energy* 96, 107093. <https://doi.org/10.1016/j.nanoen.2022.107093>.
125. Zhu, G., Zhao, C., Peng, H., Yuan, H., Hu, J., Nan, H., Lu, Y., Liu, X., Huang, J., He, C., et al. (2021). A self-limited free-standing sulfide electrolyte thin film for all-solid-state lithium metal batteries. *Adv. Funct. Mater.* 31, 2101985. <https://doi.org/10.1002/adfm.202101985>.
  126. Wang, S., Zhang, Y., Zhang, X., Liu, T., Lin, Y.H., Shen, Y., Li, L., and Nan, C.W. (2018). High-conductivity argyrodite Li<sub>6</sub>PS<sub>5</sub>Cl solid electrolytes prepared via optimized sintering processes for all-solid-state lithium-sulfur batteries. *ACS Appl. Mater. Interfaces* 10, 42279–42285. <https://doi.org/10.1021/acsami.8b15121>.
  127. Zhang, Y., Liu, T., Zhang, Q., Zhang, X., Wang, S., Wang, X., Li, L., Fan, L.Z., Nan, C.W., and Shen, Y. (2018). High-performance all-solid-state lithium-sulfur batteries with sulfur/carbon nano-hybrids in a composite cathode. *J. Mater. Chem. A*, 6, 23345–23356. <https://doi.org/10.1039/C8TA08420C>.
  128. Yang, X., Li, X., Adair, K., Zhang, H., and Sun, X. (2018). Structural design of lithium–sulfur batteries: from fundamental research to practical application. *Electrochem. Energ. Rev.* 1, 239–293. <https://doi.org/10.1007/s41918-018-0010-3>.
  129. Yang, X., Doyle-Davis, K., Gao, X., and Sun, X. (2022). Recent progress and perspectives on designing high-performance thick electrodes for all-solid-state lithium batteries. *eTransportation* 11, 100152. <https://doi.org/10.1016/j.etran.2021.100152>.
  130. Rehman, S., Pope, M., Tao, S., and McCalla, E. (2022). Evaluating the effectiveness of *in situ* characterization techniques in overcoming mechanistic limitations in lithium–sulfur batteries. *Energy Environ. Sci.* 15, 1423–1460. <https://doi.org/10.1039/D1EE03396D>.
  131. Yan, Y., Cheng, C., Zhang, L., Li, Y., and Lu, J. (2019). Deciphering the reaction mechanism of lithium–sulfur batteries by *in situ/operando* synchrotron-based characterization techniques. *Adv. Energy Mater.* 9, 1900148. <https://doi.org/10.1002/aenm.201900148>.
  132. Zhao, E., Nie, K., Yu, X., Hu, Y., Wang, F., Xiao, J., Li, H., and Huang, X. (2018). Advanced characterization techniques in promoting mechanism understanding for lithium–sulfur batteries. *Adv. Funct. Mater.* 28, 1707543. <https://doi.org/10.1002/adfm.201707543>.
  133. Wang, H., Liu, Y., Li, Y., and Cui, Y. (2019). Lithium metal anode materials design: interphase and host. *Electrochem. Energ. Rev.* 2, 509–517. <https://doi.org/10.1007/s41918-019-00054-2>.
  134. Feng, X., Fang, H., Wu, N., Liu, P., Jena, P., Nanda, J., and Mitlin, D. (2022). Review of modification strategies in emerging inorganic solid-state electrolytes for lithium, sodium, and potassium batteries. *Joule* 6, 543–587. <https://doi.org/10.1016/j.joule.2022.01.015>.
  135. Zhao, Q., Stalin, S., Zhao, C.-Z., and Archer, L.A. (2020). Designing solid-state electrolytes for safe, energy-dense batteries. *Nat. Rev. Mater.* 5, 229–252. <https://doi.org/10.1038/s41578-019-0165-5>.
  136. Manthiram, A., Yu, X., and Wang, S. (2017). Lithium battery chemistries enabled by solid-state electrolytes. *Nat. Rev. Mater.* 2, 16103. <https://doi.org/10.1038/natrevmats.2016.103>.
  137. Famprakis, T., Canepa, P., Dawson, J.A., Islam, M.S., and Masquelier, C. (2019). Fundamentals of inorganic solid-state electrolytes for batteries. *Nat. Mater.* 18, 1278–1291. <https://doi.org/10.1038/s41563-019-0431-3>.
  138. Wu, J., Yuan, L., Zhang, W., Li, Z., Xie, X., and Huang, Y. (2021). Reducing the thickness of solid-state electrolyte membranes for high-energy lithium batteries. *Energy Environ. Sci.* 14, 12–36. <https://doi.org/10.1039/D0EE02241A>.
  139. Sun, J., Yang, H., Yang, X., Chen, X., Xu, H., Shen, Y., Ding, F., Gu, X., Zhu, J., and Sun, H. (2021). Recent advances and perspectives on thin electrolytes for high-energy-density solid-state lithium batteries. *Ann. Transl. Med.* 9, 643–671. <https://doi.org/10.1039/D0EE02714F>.
  140. Balaish, M., Gonzalez-Rosillo, J.C., Kim, K.J., Zhu, Y., Hood, Z.D., and Rupp, J.L.M. (2021). Processing thin but robust electrolytes for solid-state batteries. *Nat. Energy* 6, 227–239. <https://doi.org/10.1038/s41560-020-00759-5>.
  141. Zhao, Y., Zheng, K., and Sun, X. (2018). Addressing interfacial issues in liquid-based and solid-state batteries by atomic and molecular layer deposition. *Joule* 2, 2583–2604. <https://doi.org/10.1016/j.joule.2018.11.012>.
  142. Zhao, Y., and Sun, X. (2018). Molecular layer deposition for energy conversion and storage. *ACS Energy Lett.* 3, 899–914. <https://doi.org/10.1021/acsenergylett.8b00145>.
  143. Zhao, Y., Zhang, L., Liu, J., Adair, K., Zhao, F., Sun, Y., Wu, T., Bi, X., Amine, K., Lu, J., and Sun, X. (2021). Atomic/molecular layer deposition for energy storage and conversion. *Chem. Soc. Rev.* 50, 3889–3956. <https://doi.org/10.1039/d0cs00156b>.
  144. Lin, F., Liu, Y., Yu, X., Cheng, L., Singer, A., Shpyrko, O.G., Xin, H.L., Tamura, N., Tian, C., Weng, T.-C., et al. (2017). Synchrotron X-ray analytical techniques for studying materials electrochemistry in rechargeable batteries. *Chem. Rev.* 117, 13123–13186. <https://doi.org/10.1021/acs.chemrev.7b00007>.
  145. Zhao, F., Zhang, S., Li, Y., and Sun, X. (2022). Emerging characterization techniques for electrode interfaces in sulfide-based all-solid-state lithium batteries. *Small Struct.* 3, 2100146. <https://doi.org/10.1002/sstr.202100146>.
  146. Xiang, Y., Li, X., Cheng, Y., Sun, X., and Yang, Y. (2020). Advanced characterization techniques for solid state lithium battery research. *Mater. Today* 36, 139–157. <https://doi.org/10.1016/j.mattod.2020.01.018>.
  147. Lv, C., Zhou, X., Zhong, L., Yan, C., Srinivasan, M., Seh, Z.W., Liu, C., Pan, H., Li, S., Wen, Y., and Yan, Q. (2022). Machine learning: an advanced platform for materials development and state prediction in lithium-ion batteries. *Adv. Mater.* 34, 2101474. <https://doi.org/10.1002/adma.202101474>.
  148. Liu, Y.T., Liu, S., Li, G.R., and Gao, X.P. (2021). Strategy of enhancing the volumetric energy density for lithium–sulfur batteries. *Adv. Mater.* 33, 2003955. <https://doi.org/10.1002/adma.202003955>.
  149. Huang, K.J., Ceder, G., and Olivetti, E.A. (2021). Manufacturing scalability implications of materials choice in inorganic solid-state batteries. *Joule* 5, 564–580. <https://doi.org/10.1016/j.joule.2020.12.001>.
  150. Tan, D.H., Meng, Y.S., and Jang, J. (2022). Scaling up high-energy-density sulfidic solid-state batteries: a lab-to-pilot perspective. *Joule* 6, 1755–1769. <https://doi.org/10.1016/j.joule.2022.07.002>.